

SATIN: A Multi-Task Metadataset for Classifying Satellite Imagery using Vision-Language Models

Jonathan Roberts
University of Cambridge
jdr53@cam.ac.uk

Kai Han
The University of Hong Kong
kaihanx@hku.hk

Samuel Albanie
University of Cambridge
samuel.albanie.academic@gmail.com

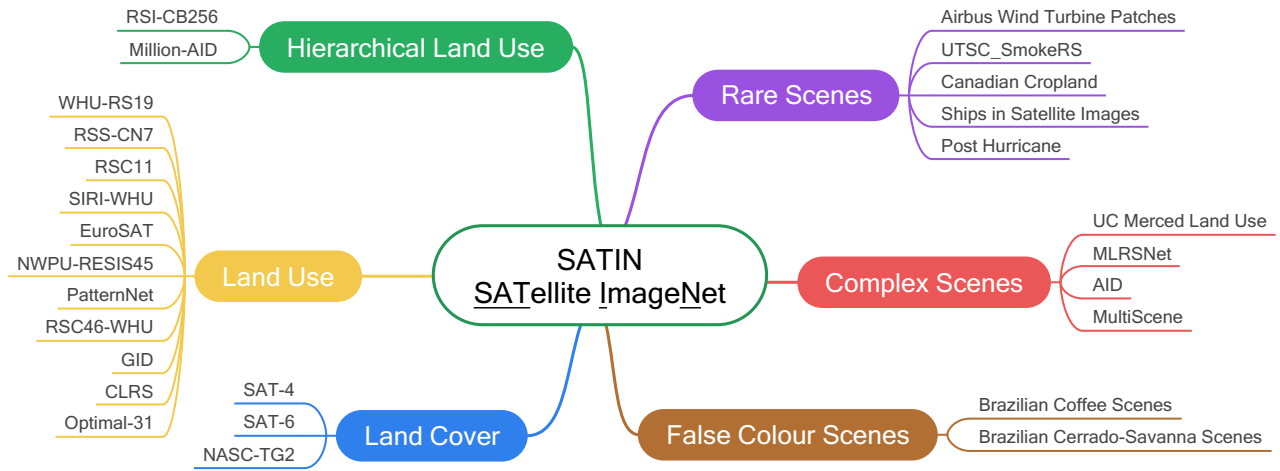


Figure 1: **The SATIN taxonomy.** We propose the SATIN benchmark containing 27 constituent datasets spanning 6 distinct tasks. The imagery is globally distributed, comprised of resolutions spanning 5 orders of magnitude and over 250 distinct class labels.

Abstract

Interpreting remote sensing imagery enables numerous downstream applications ranging from land-use planning to deforestation monitoring. Robustly classifying this data is challenging due to the Earth’s geographic diversity. While many distinct satellite and aerial image classification datasets exist, there is yet to be a benchmark curated that suitably covers this diversity. In this work, we introduce SATellite ImageNet (SATIN), a metadataset curated from 27 existing remotely sensed datasets, and comprehensively evaluate the zero-shot transfer classification capabilities of a broad range of vision-language (VL) models on SATIN. We find SATIN to be a challenging benchmark—the strongest method we evaluate achieves a classification accuracy of 52.0%. We provide a public leaderboard¹ to guide and track the progress of VL models in this important domain.

¹<https://satinbenchmark.github.io>

1. Introduction

Remote sensing (RS) of the Earth’s surface offers the potential for efficient provision of continuous sensor data at a range of temporal and spatial scales [15]. The ability to interpret this imagery yields numerous benefits and downstream applications spanning land-use planning, natural resource management and food security [60, 22] that can inform public policy [13] and enable management of environmental risk [35]. Moreover, the (near) continuous monitoring enables detection of changes such as deforestation [25], forest degradation [51], forecasting sea ice [50] and modelling urban sprawl [5].

A core component of these applications is *classification* – the ability to label an image, pixel or sub-pixel according to a set of categories. This task is challenging in the RS domain due to a number of reasons: (1) **Image diversity**—Satellite imagery, the predominant RS data source, is captured and released at a variety of fields of view and resolutions [36, 69, 77, 48, 58]. Furthermore, the global cov-

erage of satellite imagery reflects the Earth’s wide range of geographic diversity. (2) **Label hierarchies**—Land cover and land use [14] can be labeled according to different levels of abstraction: for example, a paddy field can be classed as *natural* → *agricultural land* → *arable land* → *paddy field* (e.g., [48]). (3) **Scene complexity**—The large scale of satellite imagery means that scenes can be rich in detail and include multiple different objects and land use classes. These challenges, coupled with the lack of a streamlined benchmark for RS has precluded development in this domain. Thus, there is a strong need for a satellite imagery *metadataset* – a benchmark that consists of many existing datasets grouped into key tasks – to guide the development and progress of interpreting RS imagery.

To date, the curation of a satellite imagery metadataset has been hindered by two key challenges: (i) **Models**—State-of-the-art supervised methods, such as convolutional neural networks, struggle to robustly classify satellite imagery across different domains and sets of categories, and to ingest imagery in disparate formats. Copious amounts of both compute and annotated data are required to overcome these limitations. (ii) **Data**—Datasets can be difficult to access and have inconsistent descriptions (e.g., lack key information on image resolution and geographic area). Additionally, it can be challenging to store and evaluate on multiple datasets containing different file structures, formats and other idiosyncrasies.

Due to the following recent advancements, curating an RS classification metadataset is particularly timely: (1) **VL pretraining**—The emergence of seminal open-vocabulary models such as CLIP [57] and ALIGN [34] enables zero-shot transfer: classification on unseen data distributions using natural language. This transfer paradigm obviates the need for fixed category labels, enabling a single VL model to be evaluated across a suite of tasks and datasets. (2) **Platforms & APIs**—The introduction of data and model hosting platforms and APIs (such as HF datasets [37], TF Datasets [1] and HF Transformers [73]) provide simple and inexpensive pipelines for hosting, downloading and evaluating models and datasets. (3) **RS data**—As the availability, global coverage (every few days [21]) and resolution of RS data continue to advance, there is a need for algorithms that can interpret this data accurately and robustly.

In this work, we introduce SATIN (**S**ATellite **I**mage**N**et), a metadataset curated from 27 existing datasets spanning a variety of tasks, resolutions, fields of view, and geographic areas. We leverage platforms such as HF datasets to create a streamlined benchmark that can be used and evaluated smoothly and seamlessly with minimal friction. Furthermore, we evaluate the performance of a selection of open-source VL baselines on SATIN and find that SATIN proves to be a challenging zero-shot benchmark, with even the highest capacity models scoring just above 50% accu-

racy. To encourage and keep track of progress in the RS domain, we make a public leaderboard available.

In summary, our contributions are four-fold:

- (i) We curate a challenging multi-task metadataset of remote sensing imagery;
- (ii) We collate key information on a variety of existing datasets and release them;
- (iii) We benchmark a broad profile of VL models on our metadataset, showcasing that even the best ones find it challenging;
- (iv) We provide a public leaderboard for the benchmark.

2. Related Work

Our work is related to several themes in the literature including *remote sensing classification datasets*, *metadatasets*, and *VL model evaluation*.

Remote sensing classification datasets. In recent years, numerous RS classification datasets have been released [77, 48]. Popular works include UC Merced Land Use [78], EuroSAT [30] and WHU-RS19 [75, 17], which provide a useful benchmark for machine learning models, though are relatively small and limited to a single resolution, field of view size, and geographic region. Recently, larger-scale datasets have been released with globally distributed imagery (e.g., [12, 48, 55, 16, 87, 65]) and multiple resolutions and image sizes. The SATLAS dataset [3] improves upon these with increased scale and number of labels, and by including different modalities, while it is still limited in variety of resolutions, image sizes and includes only a narrow classification task. Million-AID [48] provides an extensive land use benchmark that promotes image diversity, richness and scalability. Our SATIN metadataset agglomerates 27 of these relatively disjointed datasets, providing a comprehensive benchmark for the field of RS image classification spanning a broad range of resolutions, fields of view and tasks, and comprehensively reflects the breadth of the challenge of RS image classification.

Metadatasets. In recent years, metadatasets have emerged as useful and impactful in various fields. In natural language processing, metadatasets such as GLUE [71], SuperGLUE [70] and EleutherAI LM Harness [23] have been used to evaluate the performance of models on a range of existing datasets, allowing for a more comprehensive understanding of their strengths and limitations. Furthermore, works such as HELM [45] and BIG-bench [64] were introduced as *living benchmarks* that are updated as new scenarios, tasks, metrics and models are added. In computer vision, metadatasets such as VTAB [80], META-DATASET [68], ELEVATER [38] and NEVIS’22 [6] similarly provide an evaluation for the progress of classification models. However, META-DATASET does not include any RS datasets, and ELEVATER and VTAB only include two – both are

small-scale datasets that do not adequately reflect the diversity of the domain; NEVIS’22 also only contains two very small niche RS datasets. SATIN, on the other hand, includes 27 remote sensing datasets and is the first metadataset curated for remote sensing. One notable concurrent work is AiTLAS [18], which provides a benchmark against remote sensing classification datasets. Our work makes important distinctions in that (i) we curate a metadataset consisting of different tasks; (ii) the constituent datasets are collected and redistributed; (iii) a wide array of VL models are evaluated and a public leaderboard is further provided for tracking future progress in the RS domain.

Evaluation of VL models. The evaluation of VL classification models on remote sensing datasets has thus far been limited to the inclusion of a few remote sensing datasets as part of wider profiles of image classification datasets (most of which contain natural images), e.g., [57, 34, 38, 80, 79, 52]. Prior to our work, there has not been a broad profile evaluation of the capacity of VL models to interpret and classify remote sensing imagery.

3. SATIN Overview

The SATIN metadataset has been constructed to provide an evaluation of the capabilities of modern machine learning models on a broad range of RS image classification tasks. We intend for this benchmark to (i) primarily be used to evaluate VL models in a zero- or low-shot classification setting, and (ii) be a *living benchmark* with incremental releases offering expansions and improvements.

In the following, we detail how we build SATIN (Sec. 3.1) from multiple datasets (Sec. 3.2), what tasks are included in the benchmark (Sec. 3.3), and considered evaluation metrics (Sec. 3.4).

3.1. Design Process

SATIN has been curated from a wide set of preexisting datasets to maximally increase the variety of resolutions, field of view sizes, geographic locations, label categories and tasks. In our dataset selection, we have optimised for this diversity, and aimed to include as many datasets as possible, subject to the following constraints:

- **Licences.** We do not include datasets with research usage licencing restrictions (details given in App. A.3.1).
- **Format.** We focus on 3-channel RGB imagery, except for the *False Colour Scenes* task datasets, which include Near-Infrared, Red, Green. Some of the selected datasets include RGB and other bands, in which cases we only include the RGB imagery.
- **Platform.** Only imagery derived from satellite or airplane platforms is used, i.e., drone imagery datasets

are not included. Multi-view datasets with aerial and corresponding ‘street-level’ imagery are excluded.

- **Quality.** Based on manual visual inspection, datasets containing poor-quality imagery and/or annotations are rejected.
- **Classification.** Only datasets with image-level labels are included.
- **Size.** We avoid large datasets ($\gg 100,000$ images) as: (1) We focus on the low-shot domain, in which lower volumes are sufficient. (2) Democratisation – more of the community can benefit from a smaller-scale benchmark. (3) We increase image diversity as much as possible at a given data storage budget by having more smaller datasets rather than fewer larger ones.

3.2. Datasets

Table 1 gives details of the 27 datasets included in the SATIN metadataset. Holistically, SATIN aims to reflect the diversity in RS data by including imagery that is globally distributed, comprised of resolutions spanning from 0.06 m to 1000 m, multiple fields of view sizes, and over 250 distinct category labels. While we include the majority of the datasets used in SATIN in their entirety (regardless of pre-defined splits), for some larger datasets (denoted in the table with an *) we employ subsets defined by the dataset creators (details of the subsets we use are given in App. A.3.2).

3.3. Tasks

We group the selected datasets into 6 tasks, see Table 2 for examples of each task.²

Task 1: Land Cover. Land cover refers to the biophysical surface characteristics of the Earth (e.g., the type of vegetation or the presence of artificial structures) [19, 26]. Each image is labelled with a single broad land cover class, e.g., *forest, grassland, water or building*.

Task 2: Land Use. We distinguish land use as the economic and social functions of areas of interest [19, 14]. Each image in this task is labelled with a single land use class, which typically offers more granularity than land cover categories – *artificial structures* could be labelled as *residential* or *industrial*, or *parking lot, church* or *storage tank*; categories without a specific socioeconomic function are simply labelled as a land cover class, e.g., *water*.

Task 3: Hierarchical Land Use. This task tests the ability to classify land use across different levels of granularity. Each image is annotated with different labels depending on the level. For example, an image of a bridge could be labelled as *transportation area* \rightarrow *highway land* \rightarrow *bridge*.

²Owing to the ambiguity and overlap between ‘land use’ and ‘land cover’, the tasks should be considered ‘loose’ categorisations.

Dataset	Images in SATIN	Resolution (metres)	Image Width (pixels)	Region	Classes	Task
SAT-4* [4]	100000	1	28	N. America	4	Land Cover
SAT-6* [4]	81000	1	28	N. America	6	Land Cover
NaSC-TG2 [85]	20000	100	128	Global	10	Land Cover
WHU-RS19 [75, 17]	1013	0.5	600	-	19	Land Use
RSSCN7 [88]	2800	1 - 8 [‡]	400	Global [‡]	7	Land Use
RSC11 [83]	1232	0.2	512	N. America	11	Land Use
SIRI-WHU* [81, 82, 86]	2400	2	200	Asia	12	Land Use
EuroSAT [29, 30]	27000	10	64	Europe	10	Land Use
NWPU-RESISC45 [10]	31500	0.2 - 30	256	Global	45	Land Use
PatternNet [84]	30400	0.06 - 4.7	256	N. America	38	Land Use
RSD46-WHU* [47, 76]	117000	0.5 - 2	256	Asia [‡]	46	Land Use
GID* [67]	30000	4 [‡]	56; 112; 224	Asia	15	Land Use
Optimal-31 [72]	1860	0.2 - 1 [‡]	256	N. America [‡]	31	Land Use
CLRS [40]	15000	0.26 - 8.85	256	Global	25	Land Use
MillionAID* [48]	10000	0.2 - 153	100; 10494	Global	87	Hier. Land Use
RSI-CB256 [39]	24000	0.3 - 3	256	Global	42	Hier. Land Use
UCM Land Use [†] [78, 9]	2100	0.3	256	N. America	17	Complex Scenes
AID [†] [74, 32]	10000	0.5 - 8	600	Global	17	Complex Scenes
MLRSNet [55]	109161	0.1 - 10	256	Global	60	Complex Scenes
MultiScene* [31]	14000	0.3 - 0.6	512	Global	36	Complex Scenes
AWTP* [59]	71504	1.5	128	Global	2	Rare Scenes
Post Hurricane* [7]	10000	0.46	128	N. America	2	Rare Scenes
SISI [27]	4000	3	80	N. America	2	Rare Scenes
Canadian Cropland* [33]	14111	10	64	N. America	10	Rare Scenes
USTC-SmokeRS [2]	6225	1000	256	Global	6	Rare Scenes
BC Scenes [54]	38015	2.5 [‡]	64	S. America	2	False Colour Scenes
BCS Scenes [53]	1311	5 [‡]	64	S. America	4	False Colour Scenes

Table 1: **SATIN datasets overview.** *Images in SATIN* represents the number of images used in SATIN, not the total number in each dataset. * indicates that a subset of the dataset is used in SATIN. [†] indicates that we use a different set of labels to the original release. [‡] indicates information that was obtained/clarified via correspondence with the authors. More dataset details can be found in App. A.3.

Task 4: Complex Scenes. Given the large fields of view that remote sensing imagery can capture, many scenes contain multiple land use categories. Images used in this task contain one or more land use labels.

Task 5: Rare Scenes. For this task, imagery is classified into rare and more specialised categories that fall outside land cover and land use, e.g., *hurricane damage* or *wind turbines*, or distinguishing between different crop varieties or aerosol classes. Each image is annotated with a single category label.

Task 6: False Colour Scenes. While satellite imagery is arguably most interpretable to humans when in true-colour RGB format, additional insights can be gained by looking at other bands. For this task, we consider two datasets containing false colour images that map the near-infrared, red, green bands to red, green, blue channels. The imagery in these datasets is labelled with a single land use land cover class.

3.4. Evaluation

We use the accuracy metric to evaluate performance at three levels: *per dataset*, *per task* and *overall*.

3.4.1 Dataset Metric

Single Label. For the majority of datasets, a single ground-truth label is given per image; the dataset accuracy score is calculated as the fraction of predictions that are correct.

Multiple Labels. For images containing multiple ground-truth labels, we compare the k truth labels for a given image with the top k predicted labels; the image classification accuracy is calculated as the Jaccard Index of the lists (the number of labels occurring in both lists forms the numerator, while the number of labels across their union forms the denominator). The dataset accuracy is then calculated as the arithmetic mean over the image accuracies.

Hierarchical Labels. Where a hierarchy of labels is given per image, image classification accuracy is determined as

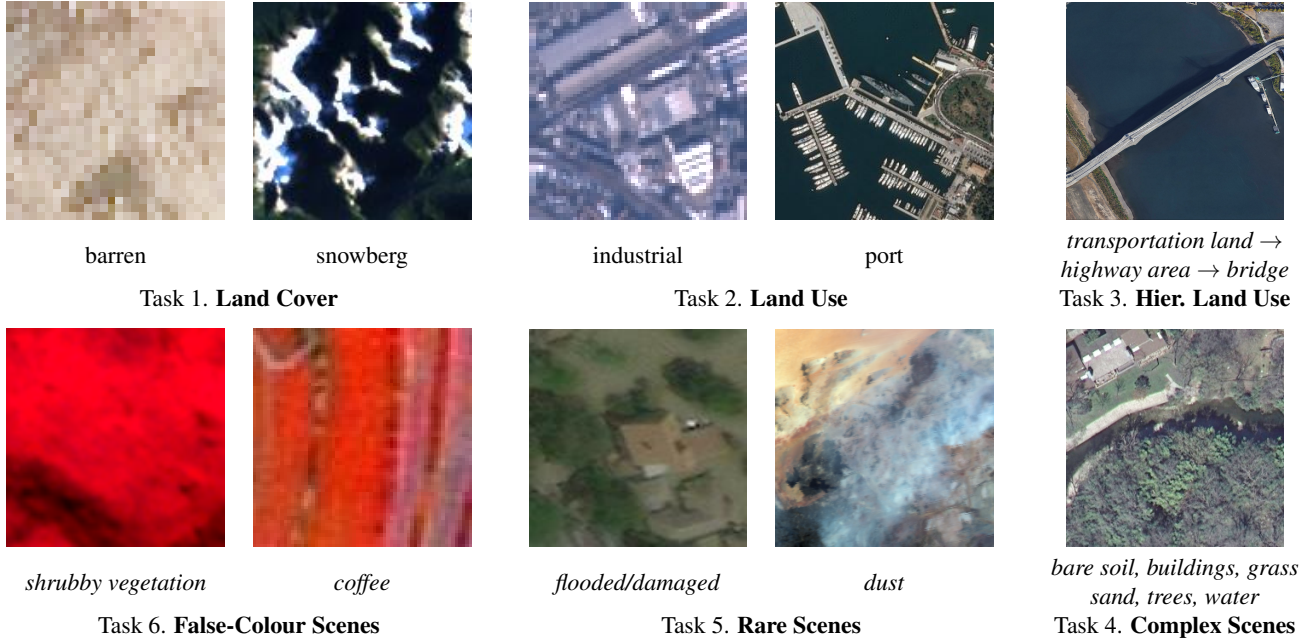


Figure 2: **Example imagery and ground truth labels for each SATIN task.** This subset includes imagery from 10 of the 27 constituent datasets and shows the breadth of diversity in SATIN across different imagery types, resolutions, fields of view and geographic areas.

the arithmetic mean in prediction accuracies at each level; the dataset accuracy is then calculated as the arithmetic mean over the image accuracies.

3.4.2 Macro-average Metrics

We take the geometric mean over the accuracy scores of the datasets for each task; this **task metric** is used to track progress across tasks and is not included in the overall SATIN metric. Due to an imbalance in the number of datasets per task, we use the geometric mean across datasets (*not tasks*) as the overall **SATIN metric**.

4. Experiments

In this section, we first describe baseline methods evaluated in our work (Sec. 4.1) and their inference procedure (Sec. 4.2). Then, we detail prompt templates used for the aforementioned tasks (Sec. 4.3) and report benchmark results (Sec. 4.4).

4.1. Baselines & Pretraining

To provide a broad overview of the capability of VL models to interpret RS imagery, we evaluate a range of open-source baselines on our SATIN metadataset. The performance of VL models varies primarily according to three major axes: (i) **Pretraining methodology**—We evaluate the following 8 pretraining methodologies on SATIN: CLIP [57], OpenCLIP [11], ALBEF [43], BLIP [42], BLIP2 [41], DeCLIP [44], SLIP [52] and CyCLIP [24]. Although CLIP

and OpenCLIP implement the same pretraining strategy (with only minor differences in configuration, e.g., batch-size and learning rate) – and therefore have no significant differences in performance given identical pretraining data – we delineate the different implementations for clarity. (ii) **Architecture**—We include a variety of sizes of ResNet-[28], ViT- [20] and ConvNeXt- [46] based image encoder backbones. (iii) **Pretraining data**—Both the quality and volume of pretraining data impacts model performance. We utilise publicly released pretrained checkpoints (details for which can be found in App. A.5) that have been created with a wide distribution of different pre-training volumes, ranging from 500K to 5.9B examples – see Table 2 for more details.

Training Size	Training Dataset(s)
500K, 1M, 2M, 2.6M	CC3M [63]
3M	CC3M [63] + CC12M [8]
14M	See [43] for details
15M	YFCC [66]
88M	DeCLIP Full Data [44]
129M	See [42] for details
400M	CLIP-WIT [57]
400M	LAION-400M [62]
2B	LAION-2B [61]
5.9B	LAION-5B [61]

Table 2: **Details of pretraining datasets.** *Training Size* denotes the number of image-text examples in the respective datasets.

Model			Zero-Shot Classification Accuracy						
Method	Backbone	Pretraining \uparrow	Task 1	Task 2	Task 3	Task 4	Task 5	Task 6	SATIN
CyCLIP [24]	RN50	3M	0.20	0.22	0.27	0.37	0.28	0.29	0.25
ALBEF [43]	ViT-B/16	14M	0.34	0.37	0.33	0.38	0.39	0.51	0.38
SLIP [52]	ViT-B/32	15M	0.30	0.22	0.19	0.29	0.36	0.22	0.26
DeCLIP [44]	ViT-B/32	88M	0.43	0.42	0.37	0.46	0.32	0.58	0.41
BLIP [42]	ViT-B/16	129M	0.37	0.50	0.45	0.50	0.37	0.46	0.45
BLIP2 [41]	ViT-G/14	129M	0.47	0.55	0.50	0.51	0.50	0.21	0.48
CLIP [57]	ViT-L/14@336px	400M	0.53	0.59	0.51	0.48	0.44	0.35	0.51
OpenCLIP [11]	ViT-G/14	2B	0.52	0.63	0.50	0.50	0.44	0.31	0.52

Table 3: **Baseline zero-shot performance on the SATIN benchmark.** For each method, we evaluate the available model with the highest capacity backbone and largest volume of pretraining data. We find that the best model achieves an overall score of just 52% on SATIN.

4.2. Inference

Steps. Although the baseline methods differ in their pre-training strategy, the steps taken by each model during inference can be generalised as the following: (1) Preprocess input images and text; (2) Extract image and text features; (3) Normalise features; (4) Compute similarity; (5) Determine top predicted class(es). See App. A.5.1 for pseudocode.

Compute. The inference time required to evaluate SATIN varies considerably depending on the model but remains practical for researchers with access to a single GPU. For instance, the BLIP model takes approximately 30 minutes to evaluate across the full SATIN benchmark with one A100 GPU. A more detailed analysis can be found in App. A.6, including inference times per dataset, per model; as well as GPU memory.

4.3. Prompt Engineering

Rather than tuning to particular datasets, we aim to provide a general overview of capability and therefore use generic prompt templates. For the majority of tasks, we use: “a satellite photo of CLS.” and “an aerial photo of CLS.”, where CLS represents the target classes. To ensure grammatical sense, we use “a satellite photo containing CLS.” and “an aerial photo containing CLS.” for the Complex Scenes task where there are one or more labels per image. To contextualise the different imagery format used in the False-Colour Scenes task, we add *false-colour* to the prompt. We take the text embedding for each target class as the average over the two prompt templates.

4.4. Benchmarking Results

Zero-shot classification results for different methods.

Table 3 shows the zero-shot classification results for each of the 8 methods, using checkpoints corresponding to the highest capacity backbones and largest volumes of pretraining images. Considering the overall SATIN metric, a general trend can be observed that performance increases with higher capacity backbones and exposure to a greater number of pretraining image-text pairs. This is in line with existing literature that has compared different backbones and

levels of pretraining, e.g., [57, 11]. The performance across the different tasks largely follows the same trend; a notable example, however, is Task 6, which sees the larger models struggling relative to those with lower capacity backbones and smaller-scale pretraining, such as the ALBEF and DeCLIP implementations. The fact that Task 6 is comprised of false-colour imagery perhaps favours models that exhibit less overfitting to natural images. Given the variation across pretraining data and backbones, this does not constitute a direct comparison of the different methods. **Key insight—***In terms of overall performance, even the largest capacity models barely surpass 50% classification accuracy, conveying that SATIN represents a challenging benchmark, suitably placed with sufficient capability in the models to significantly beat the chance score while leaving plenty of room for improvement.*

Consistency across datasets. Figure 3 provides an overview of the consistency of each method across the different datasets in the SATIN benchmark. **Key insight—***We observe a wide distribution of performance across the datasets, spanning at least 40% for each method. This spread gets larger with increasing performance as the higher capacity models attain higher scores on the easier datasets but show little improvement on a few challenging ones, such as those highlighted as outliers. An especially challenging dataset is the Canadian Cropland dataset, which contains images of 10 different crop species that are difficult for humans to distinguish (though there is sufficient information in the imagery for supervised methods to attain far beyond the chance score of 0.1 [33]). On the other hand, some datasets such as WHU-RS19 are significantly easier, with scores achieved that approach the 90% mark.*

SATIN performance wrt. pretraining. In addition to the models evaluated in Table 3, we evaluate a wider profile of method-backbone combinations at different pretraining checkpoints on SATIN, covering a total of 20 different image encoder architectures and 15 different pretraining datasets; we also include a model fine-tuned on RS data. A detailed breakdown of the per dataset scores for each model can be found in App. A.4. In Figure 4, we

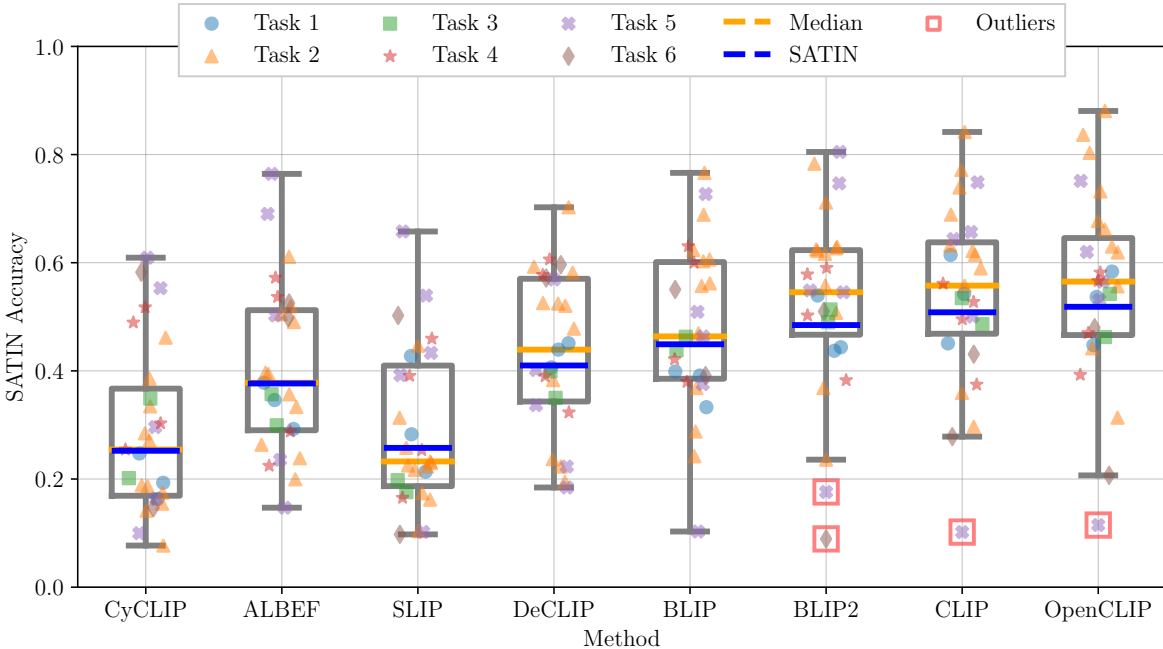


Figure 3: **SATIN task performance distribution for the models in Table 3.** A small amount of random horizontal jitter has been arbitrarily added to the scatter points to improve readability. The lowest-scoring purple cross represents the challenging Canadian Cropland dataset.

distill this performance information into a comparison of different models through the lens of pretraining image volume. **Key insight**—*Consideration of the overall distribution of points shows a general trend of increasing accuracy against the SATIN benchmark for models pretrained with a higher volume of images.* The dashed lines link models with matching methods and backbones, allowing for a more direct comparison of the effect of pretraining data. In the majority of cases, performance is correlated with the number of pretraining examples – this is especially apparent for the ALBEF (light purple crosses) and DeCLIP (light green squares) models. This can also be seen for the OpenCLIP models in the 400M and 2B regions. Despite having equivalent pretraining strategies, the CLIP 400M models noticeably outperform the corresponding OpenCLIP 400M models – as shown by the light pink, green and brown vertical dashed lines in the 400M region (representing the ViT-L/14, ViT-B/16 and ViT-B/32 backbones, respectively) – reflecting the difference in the quality of their distinct but equally sized pretraining datasets. Pretraining quality over quantity is also observable for the RN50 CLIP models in the lower data regime, where the 3M model outperforms the 12M model, which in turn outperforms the 15M model (see blue dashed line). Within the 400M and 2B regions, the higher capacity ViT models attain stronger performances, as expected.

Fine-tuning results. Given the disparity between the mostly natural images used during pretraining and in-domain RS images, it is expected that fine-tuning a model with even a relatively small volume of RS images would yield significant performance increases. We evaluate a CLIP ViT-B/32 (400M) model fine-tuned on $\sim 13K$ multi-captioned RS images³ from the RSICD [49], Sydney-captions [56] and UCM-captions [56] datasets. Despite the fact that these models have the lowest capacity ViT image encoders, the small-scale fine-tuning results in them attaining the highest scores of all the models evaluated, outperforming those with larger image encoders and volumes of pretraining data. **Key insight**—*By comparing with the equivalent model without fine-tuning we find that the absolute benefits of this fine-tuning is a performance improvement of +9.9%.* The data used during fine-tuning does include imagery (albeit with different labels) from one of the SATIN datasets, however, this represents just 1 of 27 datasets in the benchmark.

5. Broader Impacts

There are many positive applications to research involving RS data, many of which are in pursuit of achieving the UN’s SDGs⁴. Due to the nature of RS data, there is also potential for its usage in areas that are less than unanimously

³<https://huggingface.co/flax-community/clip-rsicd-v2>

⁴<https://sdgs.un.org/goals>

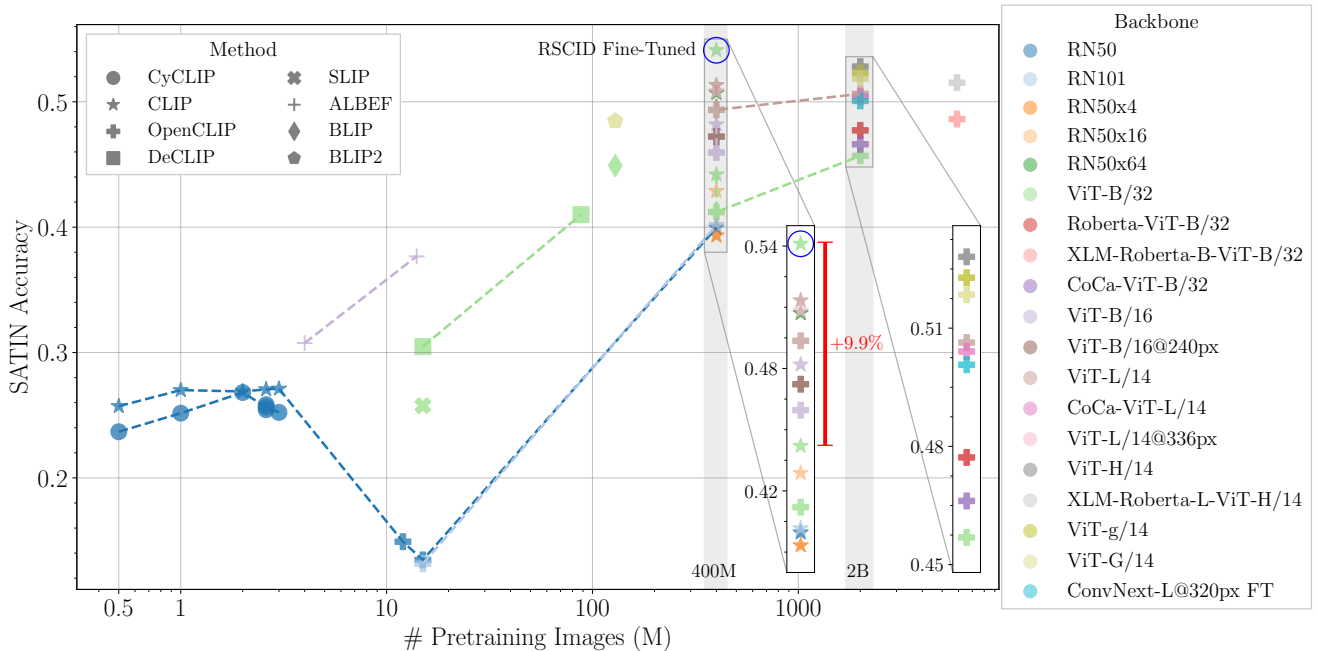


Figure 4: **SATIN zero-shot performance for a broad range of VL models.** We delineate the performance on SATIN of different models by denoting *methods* with different symbols, *backbones* with different colours, and *number of pretraining images* across the x-axis. Models with the same method and backbone are linked with dashed lines and for clarity, insets are added of the crowded regions. In general, we observe increasing SATIN accuracy with the volume of pretraining data. Of the models we benchmark, we find that a ViT-B/32 CLIP model fine-tuned with a small volume of RS data achieves the highest score.

accepted, such as surveillance.

To minimise bias and promote robustness, we aimed to maximise geographic diversity and representation within SATIN by casting a wide net and considering a broad distribution of potential constituent datasets. Despite this intention, we are still limited by the set of possible datasets that are publicly available. Although we include many globally distributed datasets, the majority of the seminal and older works tend to be limited to specific countries or continents, typically North America, Europe, and China. Furthermore, the datasets with global coverage tend to be annotated using crowdsourced platforms such as OpenStreetMap⁵ and therefore disproportionately represent locations with more users and annotations.

6. Limitations

As with many datasets involving complex scenes with large fields of view, issues arise when assigning a single classification label. While we mitigate this by including multiple labels where possible, we do not take any measures to remove background. Therefore, it might be impossible to attain 100% accuracy on some of the datasets.

In SATIN, we only use optical imagery (RGB + NIR), though some RS platforms capture imagery in other parts

⁵<https://www.openstreetmap.org/>

of the electromagnetic spectrum, such as the radio spectrum. While additional information can be garnered from these extra bands, we limit the scope of our evaluation to include optical imagery as it is closer to the distribution of images used during pre-training.

7. Conclusion

We introduce SATIN, a remote sensing image classification metadataset curated from 27 existing datasets covering a wide range of resolutions, image sizes and geographic regions, grouped into 6 different tasks. We benchmark the zero-shot classification capabilities of a broad profile of over 40 vision-language model baselines – comprising different backbones, methods and pretraining data – against SATIN. We observe that SATIN proves a challenge to even the highest capacity models trained on billions of natural images, which attain an accuracy score of just over 50%. We find a wide variation in performance on the constituent datasets within SATIN, ranging from slightly above chance score to approaching 90%. We evaluate a small number of fine-tuned models against SATIN and find significant performance increases after exposure to a relatively low number of in-domain images, though plenty of room for improvement remains. We release SATIN and provide a public

leaderboard to track progress in the development of vision-language models for remote sensing image interpretation, a domain with a multitude of socially beneficial applications.

Acknowledgements

We thank the authors of the original datasets included in SATIN for their help during the curation of our benchmark. We also thank Gyungin Shin and Vishaal Udandarao for their thoughtful comments when reviewing this manuscript.

This work was supported by the UKRI Centre for Doctoral Training in Application of Artificial Intelligence to the study of Environmental Risks (reference EP/S022961/1), an Isaac Newton Trust grant, an EPSRC HPC grant, the Hong Kong Research Grant Council - Early Career Scheme (Grant No. 27208022), and HKU Seed Fund for Basic Research. Samuel would like to acknowledge the support of Z. Novak and N. Novak in enabling his contribution.

References

- [1] TensorFlow Datasets, a collection of ready-to-use datasets. <https://www.tensorflow.org/datasets>. 2
- [2] Rui Ba, Chen Chen, Jing Yuan, Weiguo Song, and Siuming Lo. Smokenet: Satellite smoke scene detection using convolutional neural network with spatial and channel-wise attention. *Remote Sensing*, 11(14):1702, 2019. 4
- [3] Favyen Bastani, Piper Wolters, Ritwik Gupta, Joe Ferdinando, and Aniruddha Kembhavi. Satlas: A large-scale, multi-task dataset for remote sensing image understanding. *arXiv preprint arXiv:2211.15660*, 2022. 2
- [4] Saikat Basu, Sangram Ganguly, Supratik Mukhopadhyay, Robert DiBiano, Manohar Karki, and Ramakrishna Nemani. DeepSAT: a learning framework for satellite imagery. In *Proceedings of the 23rd SIGSPATIAL international conference on advances in geographic information systems*, pages 1–10, 2015. 4
- [5] Mukesh Singh Boori, Maik Netzband, Komal Choudhary, and Vít Voženílek. Monitoring and modeling of urban sprawl through remote sensing and GIS in Kuala Lumpur, Malaysia. *Ecological Processes*, 4(1):1–10, 2015. 1
- [6] Jorg Bornschein, Alexandre Galashov, Ross Hemsley, Amal Rannen-Triki, Yutian Chen, Arslan Chaudhry, Xu Owen He, Arthur Douillard, Massimo Caccia, Qixiang Feng, et al. Nevis’22: A stream of 100 tasks sampled from 30 years of computer vision research. *arXiv preprint arXiv:2211.11747*, 2022. 2
- [7] Quoc Dung Cao and Youngjun Choe. Deep learning based damage detection on post-hurricane satellite imagery. *arXiv preprint arXiv:1807.01688*, 2018. 4
- [8] Soravit Changpinyo, Piyush Sharma, Nan Ding, and Radu Soricut. Conceptual 12m: Pushing web-scale image-text pre-training to recognize long-tail visual concepts. In *Proceedings of the IEEE/CVF Conference on Computer Vision and Pattern Recognition*, pages 3558–3568, 2021. 5
- [9] Bindita Chaudhuri, Begüm Demir, Subhasis Chaudhuri, and Lorenzo Bruzzone. Multilabel remote sensing image retrieval using a semisupervised graph-theoretic method. *IEEE Transactions on Geoscience and Remote Sensing*, 56(2):1144–1158, 2018. 4
- [10] Gong Cheng, Junwei Han, and Xiaoqiang Lu. Remote sensing image scene classification: Benchmark and state of the art. *Proceedings of the IEEE*, 105(10):1865–1883, 2017. 4
- [11] Mehdi Cherti, Romain Beaumont, Ross Wightman, Mitchell Wortsman, Gabriel Ilharco, Cade Gordon, Christoph Schuhmann, Ludwig Schmidt, and Jenia Jitsev. Reproducible scaling laws for contrastive language-image learning. *arXiv preprint arXiv:2212.07143*, 2022. 5, 6
- [12] Gordon Christie, Neil Fendley, James Wilson, and Ryan Mukherjee. Functional map of the world. In *Proceedings of the IEEE Conference on Computer Vision and Pattern Recognition*, pages 6172–6180, 2018. 2
- [13] J Cihlar. Land cover mapping of large areas from satellites: status and research priorities. *International journal of remote sensing*, 21(6-7):1093–1114, 2000. 1
- [14] Alexis J Comber. Land use or land cover? *Journal of Land Use Science*, 3(4):199–201, 2008. 2, 3
- [15] Russell G Congalton, Jianyu Gu, Kamini Yadav, Prasad Thenkabail, and Mutlu Ozdogan. Global land cover mapping: A review and uncertainty analysis. *Remote Sensing*, 6(12):12070–12093, 2014. 1
- [16] Julien Cornebise, Ivan Oršolić, and Freddie Kalaitzis. Open high-resolution satellite imagery: The worldstrat dataset—with application to super-resolution. *arXiv preprint arXiv:2207.06418*, 2022. 2
- [17] Dengxin Dai and Wen Yang. Satellite image classification via two-layer sparse coding with biased image representation. *IEEE Transactions on Geoscience and Remote Sensing*, 8(1):173–176, 2011. 2, 4
- [18] Ivica Dimitrovski, Ivan Kitanovski, Dragi Koccev, and Nikola Simidjievski. Current trends in deep learning for earth observation: An open-source benchmark arena for image classification. *ISPRS Journal of Photogrammetry and Remote Sensing*, 197:18–35, 2023. 3
- [19] Vasco Diogo and Eric Koomen. Land cover and land use indicators: review of available data. *OECD green growth Paper*, 2016. 3
- [20] Alexey Dosovitskiy, Lucas Beyer, Alexander Kolesnikov, Dirk Weissenborn, Xiaohua Zhai, Thomas Unterthiner, Mostafa Dehghani, Matthias Minderer, Georg Heigold, Sylvain Gelly, et al. An image is worth 16x16 words: Transformers for image recognition at scale. *arXiv preprint arXiv:2010.11929*, 2020. 5
- [21] Oleg Dubovik, Gregory L. Schuster, Feng Xu, Yongxiang Hu, Hartmut Bösch, Jochen Landgraf, and Zhengqiang Li. Grand challenges in satellite remote sensing. *Frontiers in Remote Sensing*, 2, 2021. 2
- [22] Steffen Fritz, Linda See, and Felix Rembold. Comparison of global and regional land cover maps with statistical information for the agricultural domain in Africa. *International Journal of Remote Sensing*, 31(9):2237–2256, 2010. 1
- [23] Leo Gao, Jonathan Tow, Stella Biderman, Sid Black, Anthony DiPofi, Charles Foster, Laurence Golding, Jeffrey Hsu,

- Kyle McDonnell, Niklas Muennighoff, Jason Phang, Laria Reynolds, Eric Tang, Anish Thite, Ben Wang, Kevin Wang, and Andy Zou. A framework for few-shot language model evaluation, Sept. 2021. [2](#)
- [24] Shashank Goel, Hritik Bansal, Sumit Bhatia, Ryan A Rossi, Vishwa Vinay, and Aditya Grover. Cyclip: Cyclic contrastive language-image pretraining. *arXiv preprint arXiv:2205.14459*, 2022. [5](#), [6](#)
- [25] Clovis Grinand, Fety Rakotomalala, Valéry Gond, Romuald Vaudry, Martial Bernoux, and Ghislain Vieilledent. Estimating deforestation in tropical humid and dry forests in madagascar from 2000 to 2010 using multi-date landsat satellite images and the random forests classifier. *Remote Sensing of Environment*, 139:68–80, 2013. [1](#)
- [26] Cristina Gómez, Joanne C. White, and Michael A. Wulder. Optical remotely sensed time series data for land cover classification: A review. *ISPRS Journal of Photogrammetry and Remote Sensing*, 116:55–72, 2016. [3](#)
- [27] Robert Hammell. Ships in satellite imagery. <https://www.kaggle.com/datasets/rhammell/ships-in-satellite-imagery>, 2018. [4](#)
- [28] Kaiming He, Xiangyu Zhang, Shaoqing Ren, and Jian Sun. Deep residual learning for image recognition. In *Proceedings of the IEEE conference on computer vision and pattern recognition*, pages 770–778, 2016. [5](#)
- [29] Patrick Helber, Benjamin Bischke, Andreas Dengel, and Damian Borth. Introducing eurosat: A novel dataset and deep learning benchmark for land use and land cover classification. In *IGARSS 2018-2018 IEEE International Geoscience and Remote Sensing Symposium*, pages 204–207. IEEE, 2018. [4](#)
- [30] Patrick Helber, Benjamin Bischke, Andreas Dengel, and Damian Borth. Eurosat: A novel dataset and deep learning benchmark for land use and land cover classification. *IEEE Journal of Selected Topics in Applied Earth Observations and Remote Sensing*, 2019. [2](#), [4](#)
- [31] Y. Hua, L. Mou, P. Jin, and X. X. Zhu. Multiscene: A large-scale dataset and benchmark for multi-scene recognition in single aerial images. *IEEE Transactions on Geoscience and Remote Sensing*, in press. [4](#)
- [32] Yuansheng Hua, Lichao Mou, and Xiao Xiang Zhu. Relation network for multi-label aerial image classification. *IEEE Transactions on Geoscience and Remote Sensing*, DOI:10.1109/TGRS.2019.2963364. [4](#)
- [33] Amanda A Boatswain Jacques, Abdoulaye Baniré Diallo, and Etienne Lord. Towards the creation of a canadian land-use dataset for agricultural land classification. In *42nd Canadian Symposium on Remote Sensing: Understanding Our World: Remote Sensing for a Sustainable Future*, 2021. [4](#), [6](#)
- [34] Chao Jia, Yinfei Yang, Ye Xia, Yi-Ting Chen, Zarana Parekh, Hieu Pham, Quoc Le, Yun-Hsuan Sung, Zhen Li, and Tom Duerig. Scaling up visual and vision-language representation learning with noisy text supervision. In *International Conference on Machine Learning*, pages 4904–4916. PMLR, 2021. [2](#), [3](#)
- [35] Jeremy T. Kerr and Marsha Ostrovsky. From space to species: ecological applications for remote sensing. *Trends in Ecology & Evolution*, 18(6):299–305, 2003. [1](#)
- [36] Jhoon Kim, Ukkyo Jeong, Myoung-Hwan Ahn, Jae H Kim, Rokjin J Park, Hanlim Lee, Chul Han Song, Yong-Sang Choi, Kwon-Ho Lee, Jung-Moon Yoo, et al. New era of air quality monitoring from space: Geostationary environment monitoring spectrometer (gems). *Bulletin of the American Meteorological Society*, 101(1):E1–E22, 2020. [1](#)
- [37] Quentin Lhoest, Albert Villanova del Moral, Yacine Jernite, Abhishek Thakur, Patrick von Platen, Suraj Patil, Julien Chaumond, Mariama Drame, Julien Plu, Lewis Tunstall, Joe Davison, Mario Šaško, Gunjan Chhablani, Bhavitvya Malik, Simon Brandeis, Teven Le Scao, Victor Sanh, Canwen Xu, Nicolas Patry, Angelina McMillan-Major, Philipp Schmid, Sylvain Gugger, Clément Delangue, Théo Matussière, Lysandre Debut, Stas Bekman, Pierric Cistac, Thibault Goehringer, Victor Mustar, François Lagunas, Alexander Rush, and Thomas Wolf. Datasets: A community library for natural language processing. In *Proceedings of the 2021 Conference on Empirical Methods in Natural Language Processing: System Demonstrations*, pages 175–184, Online and Punta Cana, Dominican Republic, Nov. 2021. Association for Computational Linguistics. [2](#)
- [38] Chunyuan Li, Haotian Liu, Liunan Harold Li, Pengchuan Zhang, Jyoti Aneja, Jianwei Yang, Ping Jin, Yong Jae Lee, Houdong Hu, Zicheng Liu, et al. Elevater: A benchmark and toolkit for evaluating language-augmented visual models. *arXiv preprint arXiv:2204.08790*, 2022. [2](#), [3](#)
- [39] Haifeng Li, Xin Dou, Chao Tao, Zhixiang Wu, Jie Chen, Jian Peng, Min Deng, and Ling Zhao. Rsi-cb: A large-scale remote sensing image classification benchmark using crowd-sourced data. *Sensors*, 20(6):1594, 2020. [4](#)
- [40] Haifeng Li, Hao Jiang, Xin Gu, Jian Peng, Wenbo Li, Liang Hong, and Chao Tao. Clrs: Continual learning benchmark for remote sensing image scene classification. *Sensors*, 20(4), 2020. [4](#)
- [41] Junnan Li, Dongxu Li, Silvio Savarese, and Steven Hoi. Blip-2: Bootstrapping language-image pre-training with frozen image encoders and large language models. *arXiv preprint arXiv:2301.12597*, 2023. [5](#), [6](#)
- [42] Junnan Li, Dongxu Li, Caiming Xiong, and Steven Hoi. Blip: Bootstrapping language-image pre-training for unified vision-language understanding and generation. In *International Conference on Machine Learning*, pages 12888–12900. PMLR, 2022. [5](#), [6](#)
- [43] Junnan Li, Ramprasaath Selvaraju, Akhilesh Gotmare, Shafiq Joty, Caiming Xiong, and Steven Chu Hong Hoi. Align before fuse: Vision and language representation learning with momentum distillation. *Advances in neural information processing systems*, 34:9694–9705, 2021. [5](#), [6](#)
- [44] Yangguang Li, Feng Liang, Lichen Zhao, Yufeng Cui, Wanli Ouyang, Jing Shao, Fengwei Yu, and Junjie Yan. Supervision exists everywhere: A data efficient contrastive language-image pre-training paradigm. *arXiv preprint arXiv:2110.05208*, 2021. [5](#), [6](#)
- [45] Percy Liang, Rishi Bommasani, Tony Lee, Dimitris Tsipras, Dilara Soylu, Michihiro Yasunaga, Yian Zhang, Deepak Narayanan, Yuhuai Wu, Ananya Kumar, et al. Holistic evaluation of language models. *arXiv preprint arXiv:2211.09110*, 2022. [2](#)

- [46] Zhuang Liu, Hanzi Mao, Chao-Yuan Wu, Christoph Feichtenhofer, Trevor Darrell, and Saining Xie. A convnet for the 2020s. In *Proceedings of the IEEE/CVF Conference on Computer Vision and Pattern Recognition*, pages 11976–11986, 2022. 5
- [47] Yang Long, Yiping Gong, Zhifeng Xiao, and Qing Liu. Accurate object localization in remote sensing images based on convolutional neural networks. *IEEE Transactions on Geoscience and Remote Sensing*, 55(5):2486–2498, 2017. 4
- [48] Yang Long, Gui-Song Xia, Shengyang Li, Wen Yang, Michael Ying Yang, Xiao Xiang Zhu, Liangpei Zhang, and Deren Li. On creating benchmark dataset for aerial image interpretation: Reviews, guidances, and million-aid. *IEEE Journal of selected topics in applied earth observations and remote sensing*, 14:4205–4230, 2021. 1, 2, 4
- [49] Xiaoqiang Lu, Binqiang Wang, Xiangtao Zheng, and Xuelong Li. Exploring models and data for remote sensing image caption generation. *IEEE Transactions on Geoscience and Remote Sensing*, 56(4):2183–2195, 2018. 7
- [50] Marko Mäkynen, Jari Haapala, Giuseppe Aulicino, Beena Balan-Sarojini, Magdalena Balmaseda, Alexandru Gegiuc, Fanny Girard-Ardhuin, Stefan Hendricks, Georg Heygster, Larysa Istomina, et al. Satellite observations for detecting and forecasting sea-ice conditions: A summary of advances made in the spices project by the eu’s horizon 2020 programme. *Remote Sensing*, 12(7):1214, 2020. 1
- [51] Anthea L Mitchell, Ake Rosenqvist, and Brice Mora. Current remote sensing approaches to monitoring forest degradation in support of countries measurement, reporting and verification (mrv) systems for redd+. *Carbon balance and management*, 12(1):1–22, 2017. 1
- [52] Norman Mu, Alexander Kirillov, David Wagner, and Saining Xie. Slip: Self-supervision meets language-image pre-training. In *Computer Vision—ECCV 2022: 17th European Conference, Tel Aviv, Israel, October 23–27, 2022, Proceedings, Part XXVI*, pages 529–544. Springer, 2022. 3, 5, 6
- [53] Keiller Nogueira, Jefersson A Dos Santos, Tamires Fornazari, Thiago Sanna Freire Silva, Leonor Patricia Morelato, and Ricardo da S Torres. Towards vegetation species discrimination by using data-driven descriptors. In *2016 9th IAPR Workshop on Pattern Recognition in Remote Sensing (PRRS)*, pages 1–6. Ieee, 2016. 4
- [54] Otávio AB Penatti, Keiller Nogueira, and Jefersson A Dos Santos. Do deep features generalize from everyday objects to remote sensing and aerial scenes domains? In *Proceedings of the IEEE conference on computer vision and pattern recognition workshops*, pages 44–51, 2015. 4
- [55] Xiaoman Qi, Panpan Zhu, Yuebin Wang, Liqiang Zhang, Junhuan Peng, Mengfan Wu, Jialong Chen, Xudong Zhao, Ning Zang, and P Takis Mathiopoulos. Mlrsnet: A multi-label high spatial resolution remote sensing dataset for semantic scene understanding. *ISPRS Journal of Photogrammetry and Remote Sensing*, 169:337–350, 2020. 2, 4
- [56] Bo Qu, Xuelong Li, Dacheng Tao, and Xiaoqiang Lu. Deep semantic understanding of high resolution remote sensing image. In *2016 International Conference on Computer, Information and Telecommunication Systems (CITS)*, pages 1–5, 2016. 7
- [57] Alec Radford, Jong Wook Kim, Chris Hallacy, Aditya Ramesh, Gabriel Goh, Sandhini Agarwal, Girish Sastry, Amanda Askell, Pamela Mishkin, Jack Clark, et al. Learning transferable visual models from natural language supervision. In *International Conference on Machine Learning*, pages 8748–8763. PMLR, 2021. 2, 3, 5, 6
- [58] John Rogan and DongMei Chen. Remote sensing technology for mapping and monitoring land-cover and land-use change. *Progress in planning*, 61(4):301–325, 2004. 1
- [59] Airbus DS GEO S.A. Airbus wind turbine patches. <https://www.kaggle.com/datasets/airbusgeo/airbus-wind-turbines-patches>, 2021. 4
- [60] David Saah, Karis Tenneson, Mir Matin, Kabir Uddin, Peter Cutter, Ate Poortinga, Quyen H. Nguyen, Matthew Patterson, Gary Johnson, Kel Markert, Africa Flores, Eric Anderson, Amanda Weigel, Walter L. Ellenberg, Radhika Bhargava, Aekkapol Aekakkarungroj, Biplov Bhandari, Nishanta Khanal, Ian W. Housman, Peter Potapov, Alexandra Tyukavina, Paul Maus, David Ganz, Nicholas Clinton, and Farrukh Chishtie. Land cover mapping in data scarce environments: Challenges and opportunities. *Frontiers in Environmental Science*, 7, 2019. 1
- [61] Christoph Schuhmann, Romain Beaumont, Richard Vencu, Cade Gordon, Ross Wightman, Mehdi Cherti, Theo Coombes, Aarush Katta, Clayton Mullis, Mitchell Wortsman, et al. Laion-5b: An open large-scale dataset for training next generation image-text models. *arXiv preprint arXiv:2210.08402*, 2022. 5
- [62] Christoph Schuhmann, Richard Vencu, Romain Beaumont, Robert Kaczmarczyk, Clayton Mullis, Aarush Katta, Theo Coombes, Jenia Jitsev, and Aran Komatsuzaki. Laion-400m: Open dataset of clip-filtered 400 million image-text pairs. *arXiv preprint arXiv:2111.02114*, 2021. 5
- [63] Piyush Sharma, Nan Ding, Sebastian Goodman, and Radu Soricut. Conceptual captions: A cleaned, hypemymed, image alt-text dataset for automatic image captioning. In *Proceedings of the 56th Annual Meeting of the Association for Computational Linguistics (Volume 1: Long Papers)*, pages 2556–2565, 2018. 5
- [64] Aarohi Srivastava, Abhinav Rastogi, Abhishek Rao, Abu Awal Md Shoeb, Abubakar Abid, Adam Fisch, Adam R Brown, Adam Santoro, Aditya Gupta, Adrià Garriga-Alonso, et al. Beyond the imitation game: Quantifying and extrapolating the capabilities of language models. *arXiv preprint arXiv:2206.04615*, 2022. 2
- [65] Gencer Sumbul, Marcela Charfuelan, Begüm Demir, and Volker Markl. Bigearthnet: A large-scale benchmark archive for remote sensing image understanding. In *IGARSS 2019-2019 IEEE International Geoscience and Remote Sensing Symposium*, pages 5901–5904. IEEE, 2019. 2
- [66] Bart Thomee, David A Shamma, Gerald Friedland, Benjamin Elizalde, Karl Ni, Douglas Poland, Damian Borth, and Li-Jia Li. Yfcc100m: The new data in multimedia research. *Communications of the ACM*, 59(2):64–73, 2016. 5
- [67] Xin-Yi Tong, Gui-Song Xia, Qikai Lu, Huanfeng Shen, Shengyang Li, Shucheng You, and Liangpei Zhang. Land-

- cover classification with high-resolution remote sensing images using transferable deep models. *Remote Sensing of Environment*, 237:111322, 2020. 4
- [68] Eleni Triantafyllou, Tyler Zhu, Vincent Dumoulin, Pascal Lamblin, Utku Evci, Kelvin Xu, Ross Goroshin, Carles Gelada, Kevin Swersky, Pierre-Antoine Manzagol, et al. Meta-dataset: A dataset of datasets for learning to learn from few examples. *arXiv preprint arXiv:1903.03096*, 2019. 2
- [69] K Wagner. Geographic information systems and glacial environments. In *Past Glacial Environments*, pages 503–536. Elsevier, 2018. 1
- [70] Alex Wang, Yada Pruksachatkun, Nikita Nangia, Amanpreet Singh, Julian Michael, Felix Hill, Omer Levy, and Samuel Bowman. Superglue: A stickier benchmark for general-purpose language understanding systems. *Advances in neural information processing systems*, 32, 2019. 2
- [71] Alex Wang, Amanpreet Singh, Julian Michael, Felix Hill, Omer Levy, and Samuel R Bowman. Glue: A multi-task benchmark and analysis platform for natural language understanding. *arXiv preprint arXiv:1804.07461*, 2018. 2
- [72] Qi Wang, Shaoteng Liu, Jocelyn Chanussot, and Xuelong Li. Scene classification with recurrent attention of vhr remote sensing images. *IEEE Transactions on Geoscience and Remote Sensing*, 57(2):1155–1167, 2018. 4
- [73] Thomas Wolf, Lysandre Debut, Victor Sanh, Julien Chaumond, Clement Delangue, Anthony Moi, Pierric Cistac, Tim Rault, Rémi Louf, Morgan Funtowicz, Joe Davison, Sam Shleifer, Patrick von Platen, Clara Ma, Yacine Jernite, Julien Plu, Canwen Xu, Teven Le Scao, Sylvain Gugger, Mariama Drame, Quentin Lhoest, and Alexander M. Rush. Transformers: State-of-the-art natural language processing. In *Proceedings of the 2020 Conference on Empirical Methods in Natural Language Processing: System Demonstrations*, pages 38–45, Online, Oct. 2020. Association for Computational Linguistics. 2
- [74] Gui-Song Xia, Jingwen Hu, Fan Hu, Baoguang Shi, Xiang Bai, Yanfei Zhong, Liangpei Zhang, and Xiaoqiang Lu. Aid: A benchmark data set for performance evaluation of aerial scene classification. *IEEE Transactions on Geoscience and Remote Sensing*, 55(7):3965–3981, 2017. 4
- [75] Gui-Song Xia, Wen Yang, Julie Delon, Yann Gousseau, Hong Sun, and Henri Maître. Structural high-resolution satellite image indexing. *Symposium: 100 Years ISPRS - Advancing Remote Sensing Science*, 2010. 2, 4
- [76] Zhifeng Xiao, Yang Long, Deren Li, Chunshan Wei, Gefu Tang, and Junyi Liu. High-resolution remote sensing image retrieval based on cnns from a dimensional perspective. *Remote Sensing*, 9(7):725, 2017. 4
- [77] Zhitong Xiong, Fahong Zhang, Yi Wang, Yilei Shi, and Xiao Xiang Zhu. Earthnets: Empowering ai in earth observation. *arXiv:2210.04936*, 2022. 1, 2
- [78] Yi Yang and Shawn Newsam. Bag-of-visual-words and spatial extensions for land-use classification. In *Proceedings of the 18th SIGSPATIAL international conference on advances in geographic information systems*, pages 270–279, 2010. 2, 4
- [79] Lewei Yao, Runhui Huang, Lu Hou, Guansong Lu, Minzhe Niu, Hang Xu, Xiaodan Liang, Zhenguo Li, Xin Jiang, and Chunjing Xu. Filip: fine-grained interactive language-image pre-training. *arXiv preprint arXiv:2111.07783*, 2021. 3
- [80] Xiaohua Zhai, Joan Puigcerver, Alexander Kolesnikov, Pierre Ruysen, Carlos Riquelme, Mario Lucic, Josip Djolonga, Andre Susano Pinto, Maxim Neumann, Alexey Dosovitskiy, et al. A large-scale study of representation learning with the visual task adaptation benchmark. *arXiv preprint arXiv:1910.04867*, 2019. 2, 3
- [81] Bei Zhao, Yanfei Zhong, Gui-Song Xia, and Liangpei Zhang. Dirichlet-derived multiple topic scene classification model for high spatial resolution remote sensing imagery. *IEEE Transactions on Geoscience and Remote Sensing*, 54(4):2108–2123, 2015. 4
- [82] Bei Zhao, Yanfei Zhong, Liangpei Zhang, and Bo Huang. The fisher kernel coding framework for high spatial resolution scene classification. *Remote Sensing*, 8(2):157, 2016. 4
- [83] Lijun Zhao, Ping Tang, and Lianzhi Huo. Feature significance-based multibag-of-visual-words model for remote sensing image scene classification. *Journal of Applied Remote Sensing*, 10(3):035004–035004, 2016. 4
- [84] Weixun Zhou, Shawn Newsam, Congmin Li, and Zhenfeng Shao. Patternnet: A benchmark dataset for performance evaluation of remote sensing image retrieval. *ISPRS journal of photogrammetry and remote sensing*, 145:197–209, 2018. 4
- [85] Zhuang Zhou, Shengyang Li, Wei Wu, Weilong Guo, Xuan Li, and Guisong Xia and Zifei Zhao. Nasc-tg2: Natural scene classification with tiangong-2 remotely sensed imagery. *IEEE Journal of Selected Topics in Applied Earth Observations and Remote Sensing*, 14:3228–3242, 2021. 4
- [86] Qiqi Zhu, Yanfei Zhong, Bei Zhao, Gui-Song Xia, and Liangpei Zhang. Bag-of-visual-words scene classifier with local and global features for high spatial resolution remote sensing imagery. *IEEE Geoscience and Remote Sensing Letters*, 13(6):747–751, 2016. 4
- [87] Xiao Xiang Zhu, Jingliang Hu, Chunping Qiu, Yilei Shi, Jian Kang, Lichao Mou, Hossein Bagheri, Matthias Häberle, Yuansheng Hua, Rong Huang, et al. So2sat lcz42: A benchmark dataset for global local climate zones classification. *arXiv preprint arXiv:1912.12171*, 2019. 2
- [88] Qin Zou, Lihao Ni, Tong Zhang, and Qian Wang. Deep learning based feature selection for remote sensing scene classification. *IEEE Geoscience and Remote Sensing Letters*, 12(11):2321–2325, 2015. 4

A. Appendix

We structure this Appendix to our main paper submission as follows. First, we outline our reproducibility statement, detailing how other researchers can replicate our findings (Sec. A.1). Following this, we outline the structure, functionality and benefits of our public leaderboard (Sec. A.2). Then, we provide a more detailed overview of the constituent datasets of SATIN, including: licencing details, split information, class names, and more example imagery (Sec. A.3). Next, we present our results in more detail, with *per dataset* scores; we also include a more in-depth analysis of the performance of the CLIP model across SATIN (Sec. A.4). We follow this by providing pseudocode for our inference pipeline as well as a table containing links to the implementation scripts and checkpoints for the models that we evaluate, and a table for the prompts we used for each dataset (Sec. A.5). Finally, we give a comparison of the compute requirements for evaluating SATIN for each of the 8 methods (Sec. A.6).

A.1. Reproducibility

We curate SATIN to be a useful and easy-to-use addition for the remote sensing and wider computer vision community. As such, we aim for our work to be entirely reproducible and release SATIN via both HuggingFace and Zenodo. We make use of publicly available model checkpoints and ensure attribution to both the checkpoint and the corresponding methodology on which we based our implementation of that particular model. We outline our methodology, including our inference pipeline, prompting strategy and model selection, to allow our results and wider findings to be reproduced. Furthermore, we will release our code upon publication.

A.2. Public Leaderboard

When released, our website will be hosted using GitHub Pages featuring a design that draws inspiration from popular metadataset benchmark websites such as [GLUE](#), [SuperGLUE](#) and [SQuAD](#). The site will include: (i) a SATIN public leaderboard; (ii) code to download and use SATIN; (iii) a more detailed overview of the constituent datasets and tasks; and (iv) links to our paper, blog post, and other useful material. There are numerous benefits to hosting a website with a leaderboard: (1) **Progress tracking**—Hosting a public leaderboard conglomerates the performances of other models into a single location, allowing users to directly compare the performance of their models with existing works, without having to scour through the literature. The leaderboard is also dynamic and not restricted to the information available at the time of publication, meaning it can serve as a useful tool for tracking the progress of research in this domain. (2) **Ease of use**—The website will provide a one-stop shop for SATIN, giving easy access to the leaderboard, code, datasets and other useful information. (3) **Living benchmark**—A further benefit of the dynamic nature of a website is that it allows SATIN to be a living benchmark that is incrementally updated with expansions and improvements, and can be modified in response to feedback from the community. The combination of these three factors enables SATIN to facilitate VL research in the remote sensing domain and drive progress forwards.

A.3. Datasets

The following section outlines additional details of the constituent datasets in SATIN.

A.3.1 Licencing Details

As mentioned in the paper, we only include datasets without licence or usage restrictions that prevent them from being used for academic research. There is a wide variety of different licences attributed to each dataset and hence their downstream usage differs slightly – see Table 4 for details. Note that we do not give SATIN an overall licence as the constituent datasets hold different licences. Instead, we retain the individual licences and usage restrictions specified for each dataset.

Dataset	Licence/Usage	Source of Licence/Usage Information
SAT-4 SAT-6	Public Domain	Obtained via correspondence with author(s) + EOS
NaSC-TG2	CC BY-NC-SA 4.0	Obtained via correspondence with author(s)
WHU-RS19	CC BY 4.0	Figshare
RSSCN7	<i>For research/academic purposes</i>	Obtained via correspondence with author(s)
RSC11	<i>Free usage without licence</i>	Obtained via correspondence with author(s)
SIRI-WHU	CC BY-NC-ND	Obtained via correspondence with author(s)
EuroSAT	MIT	Obtained via correspondence with author(s)
NWPU-RESISC45	CC-BY-SA	Obtained via correspondence with author(s)
PatternNet	<i>For research purposes</i>	Obtained via correspondence with author(s)
RSD46-WHU	<i>For education/research/commercial</i>	GitHub
GID	Public Domain	Obtained via correspondence with author(s)
CLRS	<i>For academic purposes</i>	Obtained via correspondence with author(s)
Optimal-31	<i>No licence, cite paper</i>	Obtained via correspondence with author(s)
RSI-CB256	<i>For academic purposes</i>	Obtained via correspondence with author(s)
Million-AID	CC BY-NC-ND 4.0	CodaLab
UCM Land Use	Public Domain*	Obtained via correspondence with author(s) + USGS
MLRSNet	CC BY 4.0	Mendeley Data
AID	CC0 1.0 Universal	Kaggle
MultiScene	MIT	Obtained via correspondence with author(s)
Airbus Wind Turbines Patches (AWTP)	CC BY-NC-SA 4.0	Kaggle
USTC_SmokeRS	<i>For research/education</i>	Obtained via correspondence with author(s)
Canadian Cropland	Montreal Data Licence	GitHub
Ships In Satellite Imagery	CC BY-SA 4.0	Kaggle
Post Hurricane	CC BY 4.0	IEEE Dataport
BC Scenes	CC BY-NC	Obtained via correspondence with author(s)
BCS Scenes	CC BY-NC	Obtained via correspondence with author(s)

Table 4: **SATIN constituent dataset licencing and usage information.** * No restrictions except a request to include the following in derived products and data: “Map services and data available from U.S. Geological Survey, National Geospatial Program.”

A.3.2 Split Information

We use the majority of datasets in SATIN in their entirety, however, for some we use a subset – see Table 5 for descriptions of the splits used where appropriate.

Dataset	Split used in SATIN
SAT-4	<i>Test</i>
SAT-6	<i>Test</i>
SIRI-WHU	<i>Google Image Dataset</i>
RSD46-WHU	<i>Validation</i>
GID	<i>Fine Classification, Train</i>
MillionAID	<i>Train</i>
MultiScene	<i>Clean</i>
Airbus Wind Turbine Patches	<i>Validation</i>
Post Hurricane	<i>Train_Another</i>
Canadian Cropland	<i>2017</i>

Table 5: **SATIN dataset splits**. For datasets not included in this table, all splits are used.

A.3.3 Example Imagery

Figures 5–8 contain example imagery and ground truth labels for each of the constituent datasets in SATIN, ordered according to task. These examples illustrate the breadth of diversity in the SATIN benchmark.

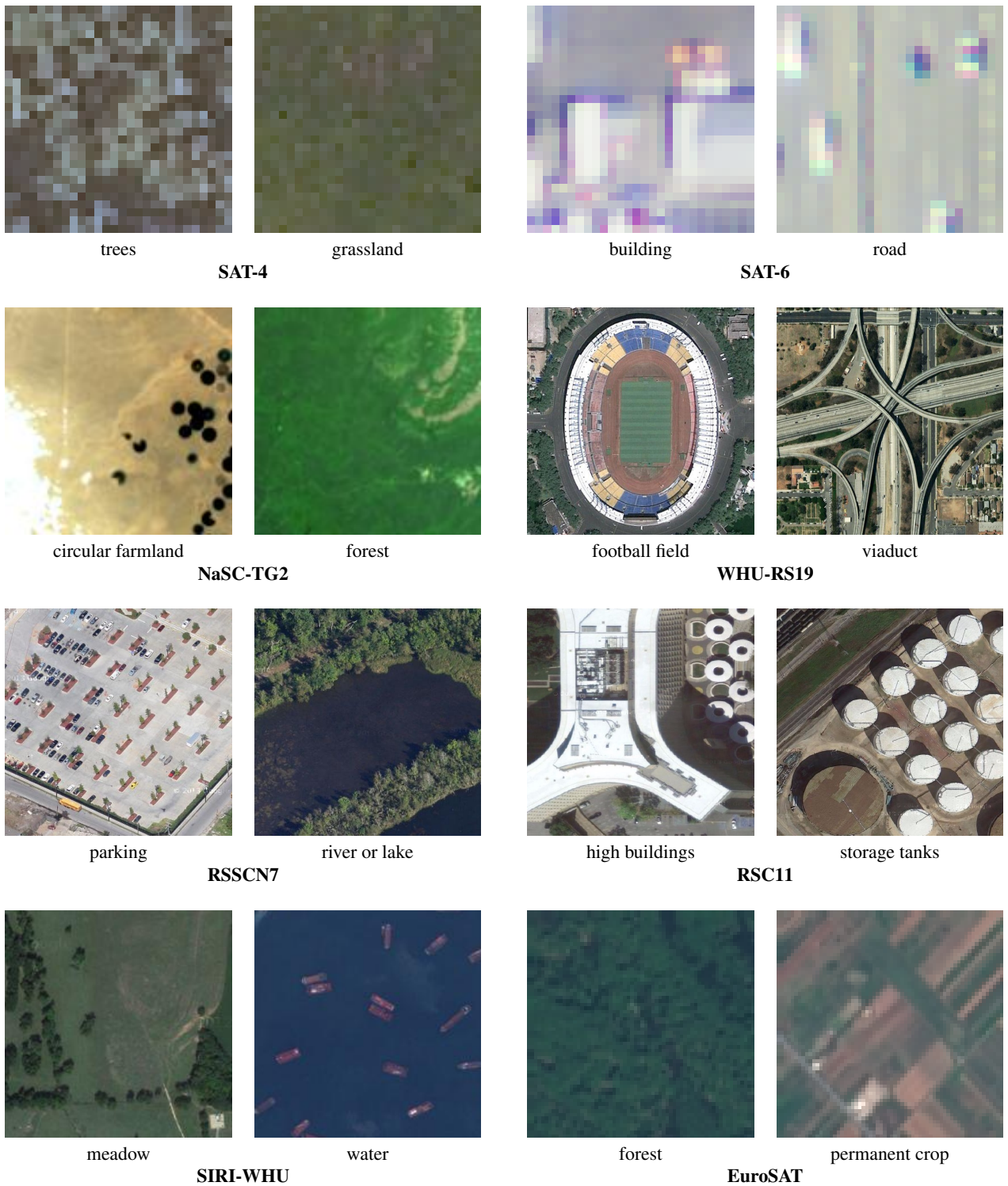
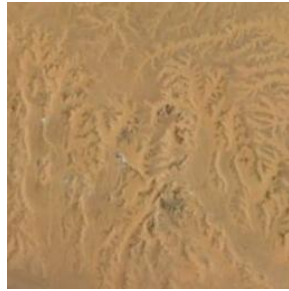


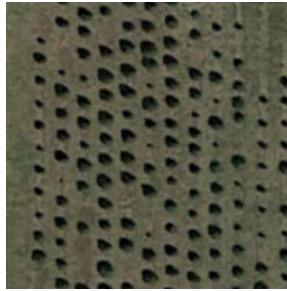
Figure 5: Example SATIN imagery and ground truth labels for *Task 1: Land Cover* (SAT-4 – NaSC-TG2) and *Task 2: Land Use* (WHU-RS19 – EuroSAT).



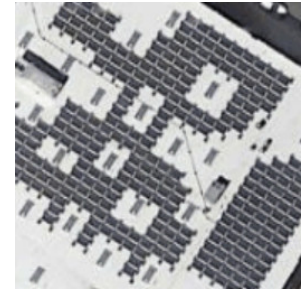
island



desert



christmas tree farm



solar panel

NWPU-RESISC45

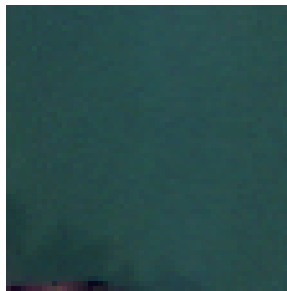
PatternNet



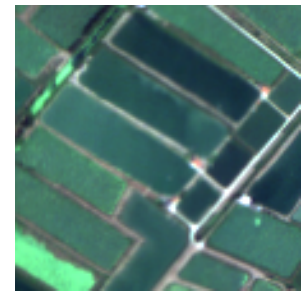
crossroads



airplane



lake



paddy field

RSD46-WHU

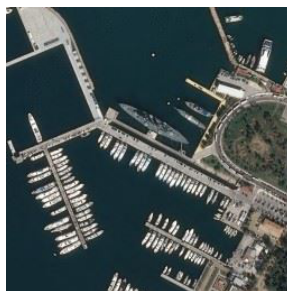
GID



golf course



dense residential



port



mountain

Optimal-31

CLRS

Figure 6: Example SATIN imagery and ground truth labels for the remaining *Task 2: Land Use* datasets.



agricultural land →
woodland → orchard

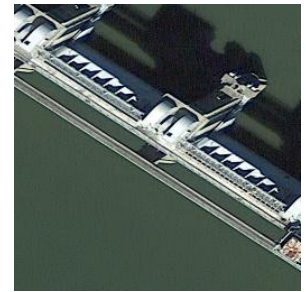


transportation land →
airport area → heliport

Million-AID



cultivated land →
dry farm

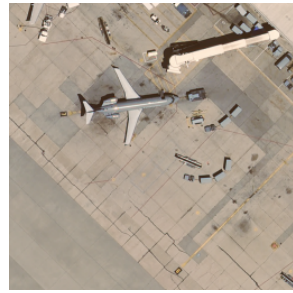


water area →
dam

RSI-CB256



bare soil, cars
pavement



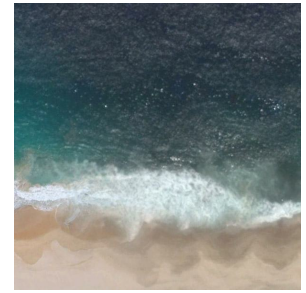
airplane, cars
pavement

UCM Land Use



buildings, cars
grass, pavement, trees

AID



sand, sea

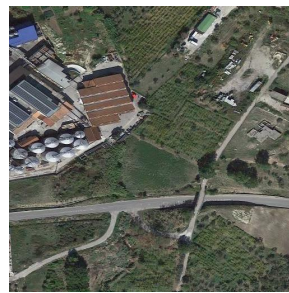


containers, pavement



field, trail
wind turbine

MLRSNet



bridge, orchard
solar panel, storage tanks, works



bridge, commercial, woodland
parking lot, railway, residential

MultiScene

Figure 7: Example SATIN imagery and ground truth labels for Task 3: Hierarchical Land Use (Million-AID – RSI-CB256) and Task 4: Complex Scenes (UCM Land Use – MultiScene).

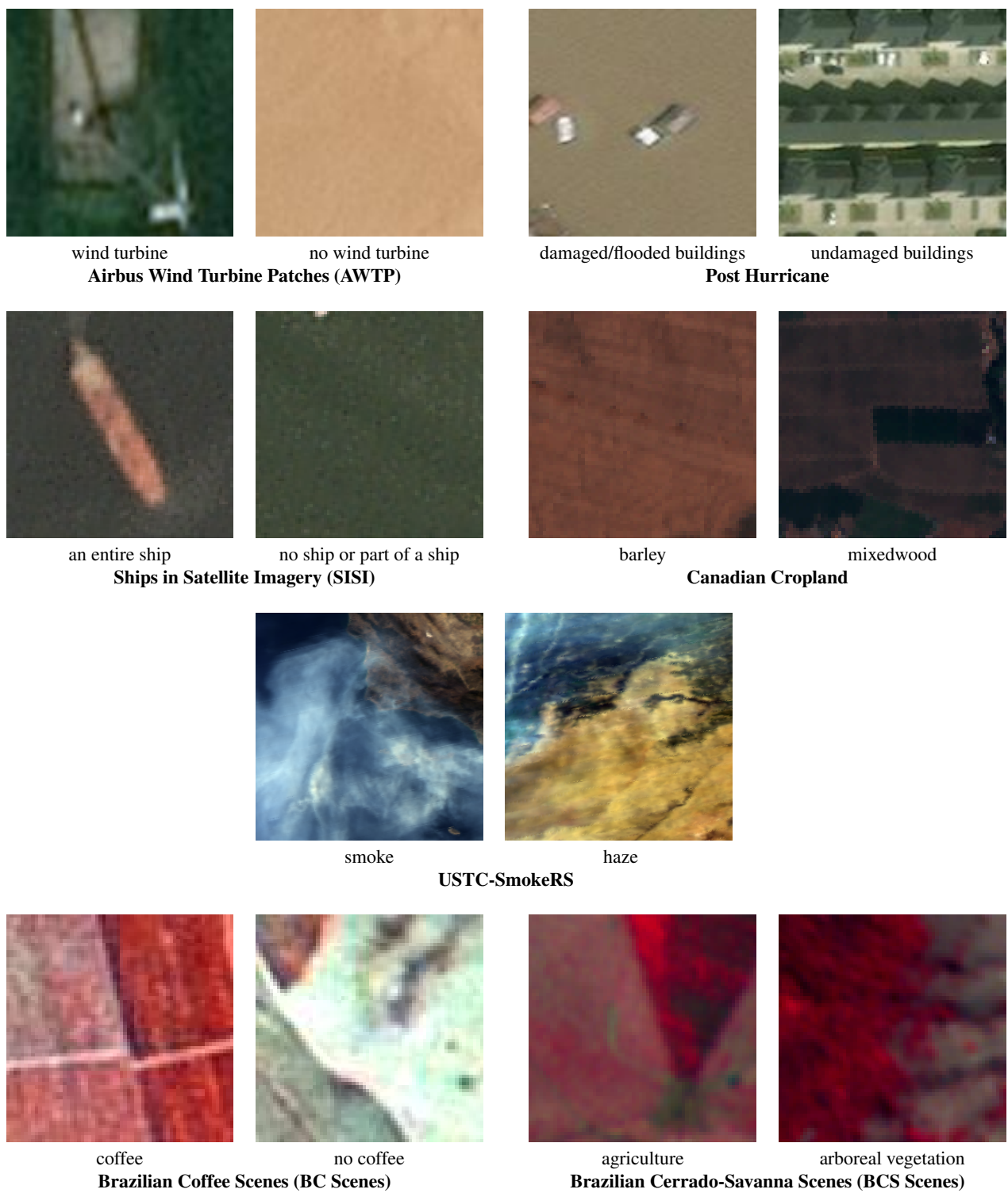


Figure 8: **Example SATIN imagery and ground truth labels** for *Task 5: Rare Scenes* (AWTP – USTC-SmokeRS) and *Task 6: False-Colour Scenes* (BC Scenes – BCS Scenes).

A.4. Results

This section presents the results for the models evaluated in the main paper in more detail. In Table 6 we include per-dataset accuracy results for each of the 8 models outlined in Table 3 of the main paper. In Table 7 we include the per-dataset accuracy results for the remaining models evaluated as part of the broad profile of VL models we benchmarked on SATIN. Tables 6 and 7 combined include the per dataset results for all the models presented in Figure 4 of the main paper. We then provide a deeper analysis of the performance on SATIN of the highest capacity CLIP model (ViT-L/14@336px, 400M) – see Figures 9, 10.

A.4.1 Per-Dataset Results

Dataset	Zero-Shot Classification Accuracy							
	CyCLIP	ALBEF	SLIP	DeCLIP	BLIP	BLIP2	CLIP	OpenCLIP
SAT-4	0.19	0.38	0.21	0.41	0.33	0.44	0.45	0.54
SAT-6	0.16	0.29	0.43	0.45	0.39	0.44	0.61	0.45
NaSC-TG2	0.25	0.35	0.28	0.44	0.40	0.54	0.54	0.58
WHU-RS19	0.33	0.61	0.26	0.70	0.77	0.78	0.84	0.88
RSSCN7	0.46	0.52	0.45	0.59	0.60	0.56	0.63	0.66
RSC11	0.39	0.50	0.31	0.52	0.62	0.51	0.62	0.63
SIRI-WHU	0.19	0.40	0.23	0.38	0.47	0.63	0.59	0.56
EuroSAT	0.14	0.26	0.23	0.22	0.37	0.63	0.56	0.62
NWPU-RESISC45	0.19	0.33	0.16	0.48	0.56	0.62	0.69	0.73
PatternNet	0.17	0.36	0.22	0.53	0.56	0.62	0.74	0.80
RSD46-WHU	0.08	0.20	0.10	0.20	0.29	0.37	0.36	0.44
GID	0.15	0.24	0.17	0.24	0.24	0.24	0.30	0.31
CLRS	0.28	0.39	0.22	0.52	0.61	0.62	0.61	0.68
Optimal-31	0.27	0.49	0.23	0.58	0.69	0.71	0.77	0.84
RSI-CB256	0.35	0.36	0.20	0.40	0.46	0.49	0.49	0.46
Million-AID	0.20	0.30	0.18	0.35	0.44	0.51	0.53	0.54
UCM Land Use	0.49	0.54	0.39	0.58	0.60	0.59	0.56	0.58
MLRSNet	0.30	0.29	0.17	0.32	0.38	0.38	0.37	0.39
AID	0.52	0.57	0.46	0.61	0.63	0.58	0.53	0.57
MultiScene	0.25	0.22	0.25	0.39	0.42	0.50	0.50	0.47
AWTP	0.55	0.50	0.43	0.40	0.38	0.55	0.66	0.57
USTC-SmokeRS	0.16	0.24	0.39	0.34	0.46	0.55	0.50	0.53
Canadian Cropland	0.10	0.15	0.10	0.18	0.10	0.18	0.10	0.11
SISI	0.30	0.76	0.66	0.22	0.73	0.75	0.75	0.75
Post Hurricane	0.61	0.69	0.54	0.57	0.51	0.80	0.64	0.62
BC Scenes	0.58	0.50	0.50	0.57	0.55	0.51	0.43	0.48
BCS Scenes	0.15	0.53	0.10	0.60	0.39	0.09	0.28	0.21
SATIN	0.25	0.38	0.26	0.41	0.45	0.48	0.51	0.52

Table 6: **Per-dataset results for the main 8 models.** Best performance on each dataset and SATIN is in **bold**. Model details are given in Table 3 of the main paper.

Model Configuration			Zero-Shot Classification Accuracy																											
Method	Backbone	Pretraining	Task 1				Task 2				Task 3				Task 4				Task 5				Task 6							
			SAT-4	SAT-6	NASC-TG2	WHU-RS19	RSSCN7	RSC11	SIRI-WHU	EuroSAT	NWPU-RESISC45	PatternNet	RSD46-WHU	GID	CLRS	Optimal-31	Million-AID	RSI-CB256	UCM Land Use	MLRSNet	AID	Multiscene	AWTP	USTC-Smokers	Canadian Cropland	SISI	Post Hurricane	BC Scenes	BCS Scenes	
CyCLIP	RN50	3M	0.19	0.16	0.25	0.33	0.46	0.39	0.19	0.14	0.19	0.17	0.08	0.15	0.28	0.27	0.20	0.35	0.49	0.30	0.52	0.25	0.55	0.16	0.10	0.30	0.61	0.58	0.15	
CLIP	RN50	3M	0.22	0.39	0.29	0.31	0.43	0.39	0.16	0.15	0.21	0.15	0.09	0.16	0.25	0.29	0.21	0.20	0.50	0.30	0.48	0.29	0.56	0.21	0.09	0.27	0.59	0.53	0.64	
CyCLIP	RN50	2.6M	0.24	0.18	0.26	0.35	0.42	0.42	0.21	0.11	0.22	0.20	0.11	0.17	0.30	0.33	0.19	0.28	0.45	0.27	0.52	0.34	0.57	0.17	0.12	0.27	0.58	0.62	0.08	
CLIP	RN50	2.6M	0.28	0.19	0.26	0.33	0.48	0.50	0.17	0.10	0.18	0.26	0.26	0.16	0.22	0.16	0.22	0.16	0.22	0.45	0.29	0.53	0.31	0.50	0.15	0.13	0.73	0.50	0.64	0.14
CyCLIP	RN50	2M	0.22	0.19	0.19	0.30	0.47	0.49	0.17	0.20	0.17	0.16	0.08	0.17	0.25	0.24	0.20	0.30	0.48	0.31	0.56	0.28	0.57	0.21	0.06	0.37	0.58	0.49	0.76	
CLIP	RN50	2M	0.24	0.20	0.30	0.29	0.41	0.48	0.24	0.23	0.19	0.16	0.09	0.21	0.24	0.27	0.20	0.30	0.42	0.23	0.50	0.30	0.57	0.20	0.09	0.41	0.68	0.48	0.19	
CyCLIP	RN50	1M	0.21	0.18	0.22	0.33	0.39	0.38	0.21	0.15	0.19	0.16	0.07	0.14	0.23	0.28	0.22	0.30	0.43	0.25	0.53	0.25	0.54	0.21	0.11	0.54	0.65	0.52	0.14	
CLIP	RN50	1M	0.20	0.47	0.24	0.27	0.41	0.41	0.20	0.21	0.17	0.13	0.08	0.19	0.18	0.24	0.19	0.28	0.40	0.27	0.49	0.28	0.56	0.17	0.07	0.72	0.57	0.52	0.72	
CyCLIP	RN50	500K	0.36	0.36	0.18	0.24	0.37	0.28	0.19	0.18	0.11	0.08	0.06	0.18	0.18	0.16	0.17	0.32	0.45	0.27	0.48	0.24	0.54	0.20	0.13	0.77	0.62	0.45	0.08	
CLIP	RN50	500K	0.28	0.39	0.22	0.23	0.38	0.28	0.22	0.19	0.14	0.11	0.07	0.16	0.19	0.18	0.17	0.31	0.44	0.26	0.47	0.25	0.37	0.21	0.17	0.63	0.58	0.62	0.41	
C-CyCLIP	RN50	2.6M	0.17	0.17	0.25	0.39	0.37	0.43	0.28	0.22	0.21	0.20	0.08	0.17	0.26	0.30	0.22	0.27	0.45	0.25	0.49	0.27	0.37	0.23	0.07	0.74	0.49	0.50	0.11	
I-CyCLIP	RN50	2.6M	0.22	0.19	0.20	0.30	0.42	0.45	0.22	0.19	0.20	0.11	0.18	0.23	0.29	0.19	0.28	0.53	0.20	0.12	0.29	0.60	0.53	0.20	0.12	0.29	0.60	0.53	0.08	
CLIP	400M	400M	0.37	0.60	0.37	0.66	0.59	0.56	0.35	0.27	0.51	0.44	0.25	0.22	0.46	0.60	0.40	0.41	0.47	0.32	0.50	0.41	0.61	0.34	0.09	0.75	0.62	0.51	0.13	
CLIP	RN101	400M	0.40	0.25	0.42	0.73	0.60	0.46	0.40	0.30	0.55	0.54	0.27	0.23	0.50	0.70	0.39	0.38	0.49	0.27	0.52	0.37	0.57	0.43	0.09	0.75	0.56	0.59	0.14	
CLIP	RN50x4	400M	0.29	0.23	0.47	0.78	0.64	0.56	0.43	0.30	0.58	0.51	0.25	0.19	0.52	0.67	0.44	0.41	0.46	0.30	0.47	0.41	0.64	0.41	0.08	0.78	0.57	0.51	0.10	
CLIP	RN50x16	400M	0.37	0.24	0.46	0.78	0.64	0.51	0.50	0.35	0.60	0.61	0.32	0.22	0.56	0.72	0.51	0.40	0.50	0.29	0.50	0.41	0.63	0.41	0.19	0.75	0.61	0.51	0.09	
CLIP	RN50x64	400M	0.44	0.48	0.44	0.81	0.67	0.64	0.55	0.44	0.66	0.65	0.35	0.23	0.53	0.75	0.54	0.44	0.54	0.38	0.55	0.47	0.73	0.39	0.16	0.76	0.51	0.56	0.73	
CLIP	VIT-B/32	400M	0.33	0.26	0.45	0.79	0.58	0.49	0.45	0.41	0.58	0.55	0.30	0.25	0.53	0.71	0.47	0.42	0.50	0.35	0.54	0.40	0.81	0.50	0.12	0.75	0.60	0.53	0.20	
CLIP	VIT-B/16	400M	0.44	0.26	0.55	0.86	0.70	0.59	0.53	0.47	0.65	0.64	0.32	0.30	0.59	0.73	0.50	0.45	0.57	0.36	0.61	0.41	0.87	0.49	0.12	0.82	0.61	0.55	0.18	
CLIP	VIT-L/14	400M	0.52	0.65	0.52	0.84	0.63	0.63	0.59	0.56	0.68	0.73	0.37	0.29	0.62	0.76	0.51	0.48	0.56	0.38	0.53	0.48	0.68	0.51	0.11	0.75	0.62	0.45	0.30	
OpenCLIP	VIT-B/16	400M	0.30	0.22	0.54	0.83	0.67	0.54	0.60	0.43	0.65	0.62	0.35	0.27	0.59	0.76	0.46	0.48	0.52	0.35	0.56	0.42	0.57	0.51	0.13	0.74	0.55	0.61	0.19	
OpenCLIP	VIT-B/16@240	400M	0.41	0.39	0.57	0.87	0.65	0.67	0.62	0.43	0.65	0.62	0.34	0.28	0.61	0.77	0.49	0.48	0.56	0.37	0.58	0.44	0.57	0.49	0.09	0.67	0.57	0.47	0.18	
OpenCLIP	VIT-L/14	400M	0.49	0.63	0.56	0.86	0.65	0.53	0.59	0.44	0.68	0.70	0.36	0.32	0.63	0.77	0.52	0.44	0.54	0.35	0.58	0.40	0.47	0.50	0.15	0.74	0.57	0.63	0.15	
OpenCLIP	VIT-L/14	2B	0.49	0.41	0.60	0.90	0.68	0.60	0.55	0.47	0.71	0.73	0.40	0.32	0.68	0.81	0.53	0.49	0.58	0.39	0.59	0.47	0.56	0.54	0.13	0.74	0.68	0.67	0.12	
OpenCLIP	CoCa-VIT-L/14	2B	0.45	0.61	0.51	0.90	0.66	0.63	0.51	0.61	0.70	0.73	0.41	0.33	0.69	0.81	0.56	0.48	0.55	0.38	0.59	0.45	0.57	0.51	0.18	0.74	0.46	0.53	0.11	
OpenCLIP	R-VIT-B/32	2B	0.43	0.40	0.48	0.86	0.69	0.61	0.55	0.50	0.62	0.66	0.32	0.32	0.61	0.73	0.49	0.50	0.51	0.35	0.54	0.43	0.58	0.43	0.19	0.75	0.61	0.55	0.11	
OpenCLIP	XLAM-R-B-VIT-B/32	5B	0.62	0.57	0.52	0.87	0.68	0.58	0.57	0.50	0.64	0.60	0.33	0.30	0.62	0.73	0.49	0.46	0.49	0.35	0.51	0.43	0.58	0.47	0.17	0.75	0.60	0.62	0.10	
OpenCLIP	CoCa-VIT-B/32	2B	0.43	0.53	0.53	0.84	0.65	0.59	0.57	0.40	0.63	0.64	0.34	0.29	0.61	0.73	0.48	0.45	0.49	0.36	0.50	0.40	0.56	0.45	0.14	0.75	0.59	0.62	0.10	
OpenCLIP	VIT-g/14	2B	0.43	0.41	0.55	0.90	0.64	0.58	0.67	0.60	0.73	0.79	0.45	0.37	0.68	0.82	0.55	0.50	0.60	0.41	0.56	0.48	0.56	0.46	0.12	0.75	0.59	0.57	0.25	
OpenCLIP	VIT-H/14	2B	0.43	0.34	0.61	0.91	0.66	0.67	0.63	0.65	0.75	0.80	0.45	0.34	0.70	0.85	0.57	0.49	0.60	0.45	0.63	0.49	0.47	0.55	0.22	0.69	0.68	0.56	0.12	
OpenCLIP	XLAM-R-L-VIT-H/14	5.9B	0.40	0.32	0.60	0.91	0.67	0.65	0.57	0.59	0.72	0.76	0.44	0.34	0.68	0.84	0.57	0.48	0.58	0.39	0.59	0.48	0.60	0.53	0.16	0.74	0.65	0.48	0.16	
CLIP	VIT-B/32 FT	400M	0.50	0.44	0.47	0.94	0.68	0.67	0.64	0.51	0.67	0.71	0.40	0.33	0.70	0.81	0.49	0.49	0.70	0.44	0.75	0.49	0.69	0.52	0.14	0.81	0.70	0.56	0.29	
OpenCLIP	RN50	15M	0.32	0.21	0.10	0.14	0.15	0.10	0.09	0.11	0.04	0.04	0.03	0.08	0.05	0.08	0.08	0.07	0.23	0.11	0.31	0.15	0.46	0.17	0.09	0.54	0.50	0.51	0.34	
OpenCLIP	RN50	12M	0.27	0.27	0.10	0.19	0.19	0.14	0.11	0.11	0.04	0.04	0.03	0.07	0.06	0.12	0.11	0.09	0.29	0.15	0.37	0.15	0.53	0.18	0.09	0.57	0.51	0.50	0.11	
OpenCLIP	RN101	15M	0.33	0.25	0.10	0.12	0.17	0.12	0.08	0.11	0.04	0.04	0.03	0.07	0.05	0.10	0.08	0.08	0.19	0.09	0.25	0.12	0.55	0.17	0.09	0.58	0.52	0.50	0.21	
OpenCLIP	VIT-B/32	400M	0.30	0.40	0.41	0.73	0.62	0.56	0.52	0.39	0.56	0.53	0.28	0.23	0.53	0.71	0.41	0.39	0.51	0.35	0.54	0.37	0.39	0.33	0.05	0.51	0.52	0.59	0.45	
OpenCLIP	VIT-B/32	2B	0.40	0.59	0.48	0.85	0.67	0.58	0.56	0.44	0.65	0.67	0.34	0.24	0.60	0.77	0.48	0.46	0.50	0.35	0.55	0.41	0.55	0.50	0.13	0.75	0.57	0.61	0.05	
OpenCLIP	CN-L@320-FT-Soup	2B	0.52	0.44	0.57	0.89	0.62	0.58	0.57	0.57	0.72	0.73	0.39	0.33	0.68	0.83	0.56	0.51	0.62	0.41	0.59	0.45	0.66	0.45	0.14	0.75	0.59	0.51	0.11	
OpenCLIP	CN-L@320-FT	2B	0.53	0.48	0.56	0.90	0.62	0.56	0.55	0.55	0.71	0.72	0.37	0.33	0.67	0.82	0.55	0.50	0.63	0.41	0.60	0.44	0.66	0.45	0.14	0.75	0.58	0.48	0.10	
ALBEF	VIT-B/16	4M	0.45	0.37	0.25	0.41	0.38	0.43	0.17	0.22	0.20	0.27	0.16	0.22	0.29	0.29	0.21	0.36	0.53	0.30	0.57	0.34	0.62	0.21	0.11	0.74	0.52	0.51	0.13	
DeCLIP	VIT-B/32	15M	0.37	0.59	0.31	0.44	0.37	0.39	0.24	0.23	0.24	0.25	0.15	0.18	0.30	0.31	0.22	0.36	0.32	0.21	0.37	0.35	0.47	0.35	0.12	0.71	0.48	0.49	0.15	

Table 7: Per-dataset results for all the remaining model configurations evaluated (see Fig. 4 in the main paper). To reduce space in the Backbone column, we abbreviate ‘Roberta’ to ‘R’ and ‘ConvNeXt’ to ‘CN’.

A.4.2 CLIP Detailed Results

Figure 9 shows the accuracy attained by CLIP against the constituent SATIN datasets. The figure further illustrates the wide distribution of performances across the SATIN datasets (10% – 84%) shown in Figure 3 in the main paper. There is also clear intra-task variability, and, to a lesser extent, inter-task variability. In Figure 10 we display confusion matrices for a dataset that CLIP performs well on (64% accuracy) and one that it performs poorly on (10% accuracy). The Canadian Cropland dataset is especially challenging because it contains different classes (crop species) that are very closely related and difficult to distinguish. The confusion matrix reflects this difficulty as almost all predictions are made against a single class, *corn*. The RSC11 dataset includes more diverse land use categories, which, in most cases, CLIP is able to tell apart. However, it can be seen to struggle on closely related classes such as *dense forest* and *sparse forest*, as well as, *overpass* and *roads*.

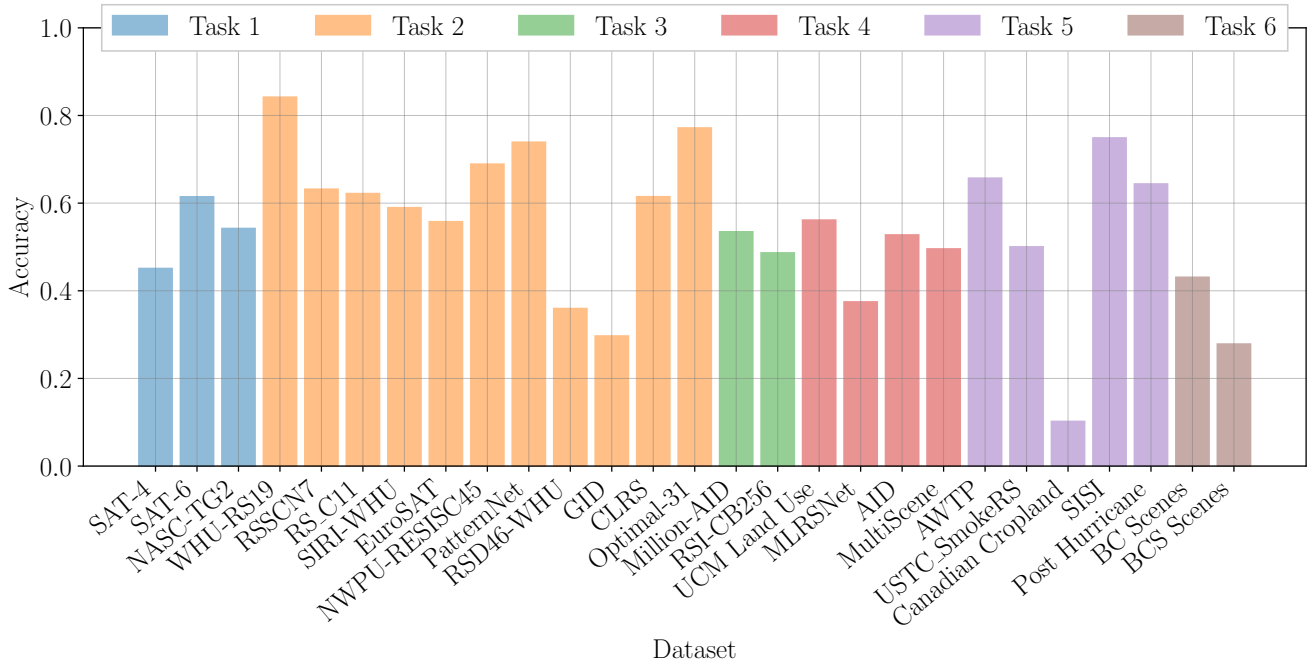


Figure 9: Per-dataset accuracy scores for the CLIP 400M ViT-L/14@336px model. Best viewed in colour.

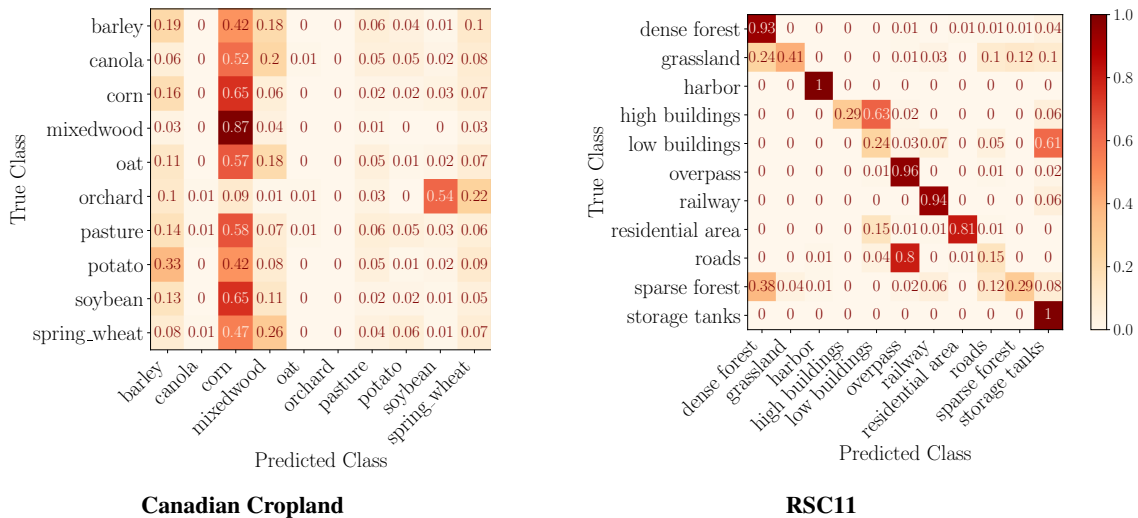


Figure 10: Confusion matrices for the CLIP ViT-L/14@336px 400M model.

A.5. Methodology

This section provides a more detailed description of the methodology we took to attain the results we presented in the main paper. Specifically, we provide PyTorch- and HuggingFace-style pseudocode for our inference pipeline in Pseudocode 1. To enable complete reproducibility, we also include links to the model checkpoints and implementation scripts that we used for each of the models we evaluated (see Table 8) as well as the exact prompt templates used per task (see Table 9).

A.5.1 Inference Pseudocode

```
# dataset_name      - SATIN dataset (e.g., EuroSAT)
# prompt_template   - Textual prompt string (e.g., "A satellite photo of ")
# k                 - Number of true labels for each image
# model             - Pretrained VL model
# processor         - Image/text pre-processor

# 0. Load data
dataset = load_dataset(path="SATIN", split=dataset_name) # download dataset
images = dataset.features["image"] # extract images from dataset
labels = dataset.features["label"] # extract labels from dataset
class_names = dataset.features["label"].names # extract class names

# 1. Preprocess input images and text
text_prompts = [prompt_template + c for c in class_names] # convert to prompts
text_inputs = processor(text=text_prompts)
image_inputs = processor(images=images)

# 2. Extract image and text features
text_features = model.get_text_features(**text_inputs)
image_features = model.get_image_features(**image_inputs)

# 3. Normalise features
text_features /= text_features.norm(dim=-1, keepdim=True)
image_features /= image_features.norm(dim=-1, keepdim=True)

# 4. Compute similarity
similarity = (100.0 * image_features @ text_features.T).softmax(dim=-1)
_, indices = similarity.topk(k)

# 5. Determine top predicted class(es)
# Correct predictions if indices == label
```

Pseudocode 1: PyTorch- and HuggingFace-style pseudocode outlining the general procedure for inference on SATIN. For particular models or implementations, steps 1 and 2 vary slightly in syntax but the functionality taken at each step remains the same. The comment numbers refer to the inference steps outlined in the main paper.

A.5.2 Model Checkpoints

Method	Backbone	Pretraining	Checkpoint source
CyCLIP, CLIP, I/C-CyCLIP	RN50	500K – 3M	https://github.com/goel-shashank/CyCLIP
CLIP	All remaining	400M	https://github.com/openai/CLIP
OpenCLIP	ConvNeXt-based	12M – 5B	https://huggingface.co/laion
OpenCLIP	All remaining	12M – 5B	https://github.com/mlfoundations/open_clip
ALBEF	ViT-B/16	4M	https://github.com/salesforce/ALBEF
ALBEF	ViT-B/16	14M	https://github.com/salesforce/LAVIS
BLIP	ViT-B/32	129M	https://github.com/salesforce/LAVIS
BLIP2	ViT-G/14	129M	https://github.com/salesforce/LAVIS
DeCLIP	ViT-B/32	15M, 88M	https://github.com/Computer-Vision-in-the-Wild/Elevater_Toolkit_IC
SLIP	ViT-B/32	15M	https://github.com/Computer-Vision-in-the-Wild/Elevater_Toolkit_IC
CLIP Fine-tuned	ViT-B/32	400M + 13K	https://huggingface.co/flax-community/clip-rs1cd-v2

Table 8: **Model checkpoints.** We provide a link for checkpoint and implementation scripts for each of the models we evaluated.

A.5.3 Prompt Templates

Task	Prompts
Task 1. Land Cover	“a satellite photo of {CLS}” “an aerial photo of {CLS}”
Task 2. Land Use	“a satellite photo of {CLS}” “an aerial photo of {CLS}”
Task 3. Hierarchical Land Use	“a satellite photo of {CLS}” “an aerial photo of {CLS}”
Task 4. Complex Scenes	“a satellite photo containing {CLS}” “an aerial photo containing {CLS}”
Task 5. Rare Scenes	“a satellite photo of {CLS}” “an aerial photo of {CLS}”
Task 6. False-colour Scenes	“a false-colour satellite photo of {CLS}” “a false-colour aerial photo of {CLS}”

Table 9: **Prompt templates.** Inference was carried out on all the datasets in a given task using the same prompt templates.

A.6. Compute Requirements

For all of our experiments, we carried out inference on a single Nvidia A100-80GB GPU with a batch size of 128. For each of the models evaluated in Table 3 of the main paper, we benchmark the inference time and maximum GPU memory required when evaluating across the entire SATIN benchmark (see Table 10). Additionally, we further provide the per-dataset inference times taken for each model (see Table 11). Note, as with the accuracy results outlined in this supplementary material and in the main paper, different model configurations are used for the different methods, therefore this analysis does not offer a direct comparison between the relative compute requirements of the different methods.

Method	Backbone	Inference Time (minutes)	GPU Memory (GB)
CyCLIP	RN50	30.6	5.02
ALBEF	ViT-B/16	25.6	5.14
SLIP	ViT-B/32	17.2	3.63
DeCLIP	ViT-B/32	18.5	3.30
BLIP	ViT-B/16	26.8	4.97
BLIP2	ViT-G/14	106.3	11.79
CLIP	ViT-L/14@336px	127.0	8.41
OpenCLIP	ViT-G/14	155.4	17.42

Table 10: Compute requirements of inference on SATIN for each of the methods evaluated in this work.

Dataset	Inference Time (seconds)							
	CyCLIP	ALBEF	SLIP	DeCLIP	BLIP	BLIP2	CLIP	OpenCLIP
SAT-4	118.8	143.0	59.7	60.0	144.9	882.5	1073.4	1389.8
SAT-6	97.4	115.4	48.5	52.1	121.0	720.8	873.9	1158.4
NaSC-TG2	35.5	38.5	21.0	26.3	43.4	198.9	233.8	276.6
WHU-RS19	12.4	12.2	12.3	17.5	18.0	27.9	33.6	24.0
RSSCN7	28.7	19.2	17.1	22.6	23.7	47.0	54.1	52.1
RSC11	35.3	10.6	10.9	14.6	14.8	27.7	31.1	25.5
SIRI-WHU	14.6	14.3	13.3	18.2	19.3	40.8	45.6	43.2
EuroSAT	39.9	45.6	22.9	28.6	51.1	252.3	304.8	368.7
NWPU-RESISC45	79.6	74.5	48.7	50.8	77.0	313.2	376.4	456.7
PatternNet	125.0	98.9	72.6	74.1	96.0	327.5	386.8	471.4
RSD46-WHU	151.9	98.2	86.3	83.2	97.0	229.1	265.5	313.9
GID	101.1	69.3	45.0	48.7	70.6	294.3	355.6	439.9
CLRS	131.2	48.8	36.9	38.4	47.4	166.9	195.1	228.9
Optimal-31	17.8	12.8	12.1	16.7	15.9	31.8	37.3	35.4
RSI-CB256	132.1	72.7	52.3	52.4	70.6	258.8	307.2	365.7
Million-AID	75.1	65.8	59.3	64.1	71.4	147.4	163.8	186.7
UCM Land Use	21.3	16.8	16.0	16.8	20.0	36.9	40.0	42.9
MLRSNet	228.0	239.7	149.7	146.6	243.8	1052.6	1262.3	1561.6
AID	30.0	31.2	30.6	33.3	33.4	59.4	63.3	71.0
MultiScene	94.0	69.3	61.0	60.9	71.0	175.9	204.9	241.7
AWTP	104.9	121.9	62.5	64.5	121.0	653.2	789.2	980.7
USTC-SmokeRS	54.1	24.8	20.4	24.6	25.9	75.6	89.8	98.7
Canadian Cropland	31.4	30.5	20.1	24.6	33.4	139.9	169.0	204.0
SISI	22.5	15.7	13.2	17.9	18.4	50.4	60.2	65.3
Post Hurricane	24.8	24.6	17.5	21.7	28.3	103.2	124.8	144.8
BC Scenes	15.6	13.1	11.7	16.8	15.7	39.7	46.1	47.0
BCS Scenes	13.2	10.8	11.3	15.5	14.0	26.2	30.1	26.9

Table 11: Per-dataset inference times for the models outlined in Table 10.